Quantifying corrosion in volcanic ash and gas environments

Prepared by: Carol Stewart[1], Zhengwei Li[2], Anna de Raadt[2] and Kelvin Tapuke[1]

1 Massey University, 2 BRANZ Ltd

c.stewart1@massey.ac.nz, Zhengwei.li@branz.co.nz

June 2026

With funding support from

Natural Hazards Commission
Toka Tū Ake

BRANZ

MASSEY UNIVERSITY
TE KUNENGA KI PŪREHUROA
UNIVERSITY OF NEW ZEALAND

Acknowledgements

We thank the Natural Hazard Commission Toka Tū Ake for funding this project as NHC Biennial 2024-075 and our institutions Massey University and BRANZ Ltd for supporting this work.

We also thank Melissa Notman and Neil Kerrison for access to the study site at the Rotorua Wastewater Treatment Plant and Ben Alton of Rotorua Airport for access to the study site on the grounds of Rotorua Airport.

We thank Shane Iremonger of Bay of Plenty Regional Council for helpful discussions about measurements of air quality in Rotorua, and Kim Smith and Darrell Holder of Rotorua Lakes Council for their interest in the project.

Executive summary

Volcanic ash and gas are important natural hazards in Aotearoa New Zealand. Future eruptions could affect buildings and infrastructure over wide areas, including locations far from the erupting volcano. While the effects of ash loading are reasonably well understood, much less is known about how volcanic gases and ash together can damage metallic building materials through corrosion. This project was designed to fill that gap and provide practical evidence to support better material specification, risk reduction, resilience planning, and decision-making for the built environment.

This project focused on a simple but important question: how do volcanic ash and gases, separately and in combination, affect the durability of common metallic building metals? To answer this, the research team carried out field exposure testing in Rotorua over one year using five representative materials: carbon steel, copper, galvanised steel, aluminium-zinc alloy coating, and quartz zinc. Exposure conditions of gas-only, ash-only, and ash plus gas, were used to investigate interactions between ash and gas. In addition, two different volcanic ashes with contrasting properties were used.

The results derived from corrosion rate measurements and morphological observations show that corrosion can begin very quickly in volcanic environments. The most vulnerable material in this study was carbon steel. It corroded very rapidly when exposed to geothermal gas, and even more quickly when volcanic ash and geothermal gas acted together in the early stage of exposure. Ash on its own also increased corrosion in the initial stage of field exposure, even at the site with little or no gas. Galvanised steel also showed faster corrosion in the short term when ash was present on its surface, but this effect reduced rapidly over time. Aluminium-zinc alloy coating and quartz zinc performed much better overall, with only limited or no measurable damage from ash under the conditions tested. Copper was strongly affected by geothermal gas but was less affected by volcanic ash. In fact, the results of this study indicate that volcanic ash surface coverage may slightly reduce the corrosion rate of copper, possibly by limiting direct contact between the copper surface and corrosive gases in the air.

An important finding was that the effect of ash was strongest in the first days and weeks after it was deposited. In this study, most ash was washed off the material surfaces by rainfall within a few days because the coupons were mounted at a 45-degree angle. Even so, that short period of ash contact was able to accelerate corrosion of some metals, especially carbon steel and, to a lesser extent, galvanised steel. This means the early period after ashfall may be critical for limiting damage. Its duration is likely to depend strongly on the prevailing climatic conditions, particularly the amount and frequency of rainfall immediately following ashfall.

Volcanic ash and gas can affect the durability of some common metallic building materials, and that the level of risk varies strongly by material type, surface condition, and their inherent corrosion resistance. This research found that new, unprotected carbon steel is the most at risk. Galvanised steel can also be affected, especially soon after ashfall. More resistant materials, such as aluminium-zinc alloy coating and quartz zinc, may perform better in these environments.

The main practical recommendation from this research is that volcanic ash should be removed from metallic building surfaces as soon as it is safe and practical to do so, particularly from vulnerable materials and especially where gases may also be present. This research also suggests that future research and resilience planning should consider not only the amount of ash deposited, but also what materials are used, how long ash remains on surfaces, how much rain falls soon after eruption, the angle of roofs and cladding, and whether materials are old and their surfaces are already roughened by weathering or corrosion. These factors are likely to influence how much damage occurs in real buildings.

Overall, this project provides an important step toward a more complete understanding of volcanic impacts on the corrosion and durability of building materials and the resilience of built environment in Aotearoa. It offers practical evidence that can help communities, asset owners, engineers, and decision-makers reduce corrosion damage, improve recovery planning, and strengthen the resilience of buildings and infrastructure in areas exposed to volcanic ash and gas.

This research is directly relevant to the Natural Hazards Commission Toka Tū Ake's focus on reducing natural hazard risk and supporting better decisions. It provides new evidence about how volcanic emissions can damage buildings and infrastructure, helps improve understanding of the vulnerability of the built environment, and supports the development of better hazard and loss models. The findings can also inform material selection, maintenance planning, and specific engineering design in volcanic and geothermal environments, including input to standards and guidance used by the building and construction sector in New Zealand.

Abstract

This project quantified the corrosion behaviour of typical metallic building materials exposed to geothermal emission volcanic ash, and their combined effects, with the aim of improving understanding of the durability of Aotearoa New Zealand's built environment in volcanic environments. The study combined one-year field exposure testing in the Rotorua Geothermal Field with laboratory characterisation to assess corrosion initiation, time-dependent corrosion behaviour, and material-specific responses.

Field exposure was conducted at two sites: a high-gas site at the wastewater treatment plant near the south end of Sulphur Bay and a low/no-gas site at Rotorua Airport. Five metallic materials were investigated: carbon steel, copper, hot-dipped galvanised zinc coating (HDG), 55 wt.% Al-Zn alloy coating, and quartz zinc. Exposure conditions of gas-only, ash-only, and ash plus gas, were used to investigate interactions between ash and gas. In addition, two different volcanic ashes with contrasting properties were used. Materials were retrieved after ~1 week, 1 month, 3 months, and 12 months.

The results show that corrosion can initiate rapidly in both geothermal gas and volcanic ash-bearing environments. Carbon steel was the most affected material, with very high early-stage corrosion rates under combined ash and gas exposure and substantial first-year corrosion under all high-gas conditions. At the low/no-gas site, ash alone also accelerated the initial corrosion of carbon steel, although corrosion rates decreased over time. Copper showed strong sensitivity to volcanic gases but comparatively limited sensitivity to ash, while HDG experienced short-term ash-induced acceleration that diminished as ash was removed. In contrast, Al-Zn alloy coating and quartz zinc showed only minor or no measurable adverse effects from ash deposition under the exposure conditions tested.

A key finding is that the influence of volcanic ash was most important during the initial stage of exposure, because most ash deposits were washed from the 45° inclined surfaces by rainfall within the first few days. Even so, ash significantly accelerated corrosion of susceptible materials, particularly carbon steel and, to a lesser extent, HDG. These results indicate that post-eruption ash removal from vulnerable metallic building components is important for reducing corrosion risk, and that material selection is critical for improving resilience in volcanic and geothermal environments. In general, a material with high inherent atmospheric corrosion resistance will be less susceptible to the effects of ash surface coverage.

Keywords

Quantifying hazards and risk, supporting people and decisions, volcanic ash and gas, building materials, corrosion, durability

Introduction

Six volcanoes have erupted within the last 200 years in Aotearoa. Within the next 50 years, the probabilities of a large eruption are >50% for Ruapehu and Whakaari and ~30-40% for Taranaki, Ngauruhoe and Tongariro, posing a major, credible threat to populations, infrastructure and buildings (Bebbington et al., 2018). Future eruptions in the Auckland Volcanic Field (AVF) and the Ahi Tupua caldera complex are expected to be less frequent but would be highly consequential.

Volcanic ash and gas emissions are far-reaching hazards and can affect large downwind areas, potentially for years to decades. While impacts of ash loading on buildings are reasonably well-characterised, much less is known about the effects of volcanic emissions on metallic building materials, which include the acceleration of corrosion. This project was designed to fill that gap and provide practical evidence-based advice to support better material specification, risk reduction, resilience planning, and decision-making for the built environment.

While there have been several previous studies of corrosion in volcanic or geothermal environments (Oze et al., 2014; Li et al., 2018), none have investigated interactions of ash and gases – which commonly co-occur in volcanic plumes – on exposed building materials. Other under-researched aspects are the relative performance of common building materials exposed to volcanic ash and gas, and timescales for the initiation of corrosion for metallic building materials exposed to volcanic emissions. The speed of onset is important for informing advice to building owners on the urgency of removing ash.

The objective of this project was to quantitatively assess how ash and gas emissions from future Aotearoa eruptions will impact the durability of our buildings and infrastructure. Our approach involves field exposure testing of common metallic building materials. Our experimental design addressed the following research questions:

- How rapidly is corrosion initiated in volcanic gas and ash environments?
- How do interactions between volcanic gas and ash affect corrosion?
- How well do different materials perform in volcanic ash and gas environments?

Methodology

Experimental design and site identification

To investigate the research questions, the following variables were included in the experimental design (Table 1): exposure duration, exposure to volcanic ash and gas separately and together and the nature of the volcanic ash.

Table 1 Experimental design

Site	Exposure condition	Exposure duration: coupons retrieved after:				Environmental monitoring	
		~1 weeks	1 month	3 months	1 year	Meteorological	Gas
Site 1 (high gas)	Gas only	X	X	X	X	Temperature, relative humidity, rainfall, wind speed, wind direction, solar radiation	Continuous and periodic gas monitoring
	Gas plus salty ash	X	X	X	X		
	Gas plus acidic ash	X	X	X	X		
Site 2 (low/no gas)	Salty ash only	X	X	X	X		Periodic gas monitoring
	Acidic ash only	X	X	X	X		
	No ash or gas	Information obtained from previous BRANZ study					

We made an early decision to base the study in Rotorua as the only location exposed to volcanic gas emissions where it would be logistically feasible to carry out a field trial. On 23 May 2024, two of the team (ZL and CS) visited Rotorua for scoping of the exact locations. Sites visited included the SCION campus and the Rotorua wastewater treatment plant (WWTP) at Te Ngae Rd, on the southern side of Sulphur Bay. A site close to a fumarole on the SCION campus was excluded from further consideration due to difficult access and hazardously high (> 30,000 µg/m^3) H_2S concentrations.

For our primary, 'high gas' site (Site 1) we chose a site within the grounds of the WWTP (Figure 1). This site is securely fenced, had H_2S concentrations that did not exceed 5000 µg/m^3 H_2S during our visit, and had some pre-existing corrosion support racks from earlier BRANZ work. For our secondary 'low to no gas' site (Site 2, Figure 1) we chose a secure site on the grounds of Rotorua airport, making use of pre-existing support racks and a BRANZ weather station. H_2S remained below 10 µg/m^3 at this site throughout our field visits.

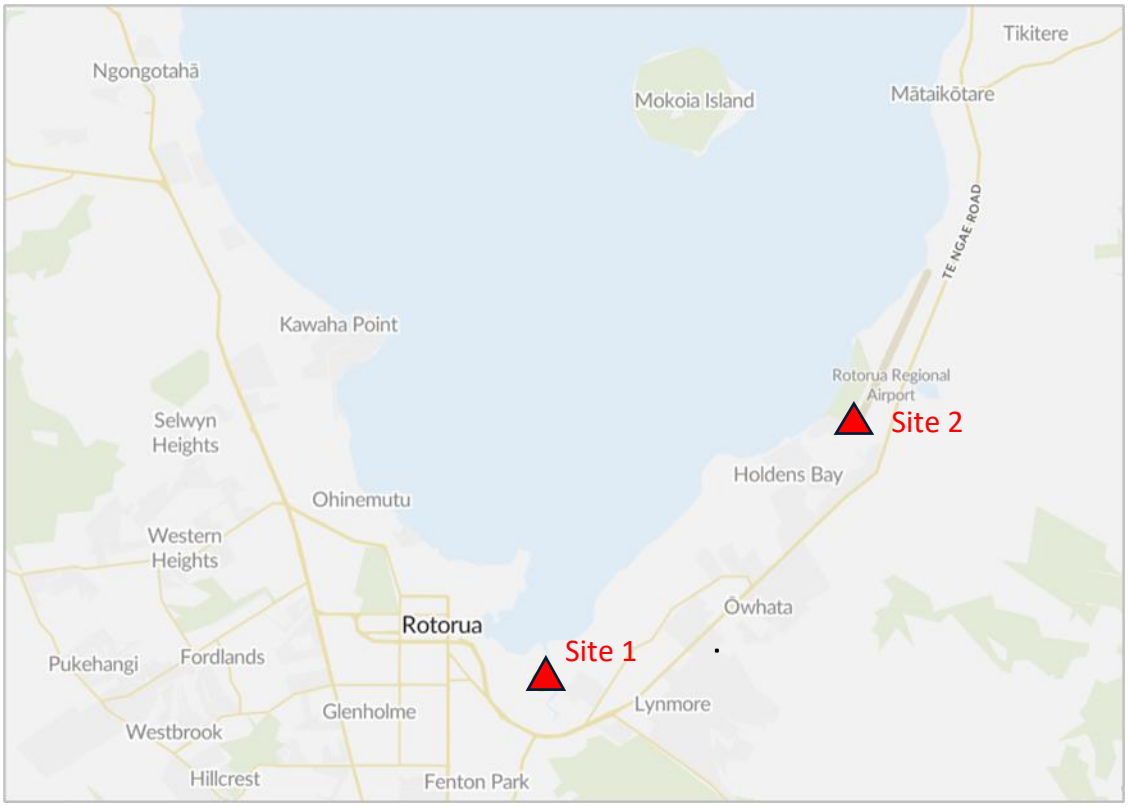

Figure 1 Location of study sites in Rotorua

Preparation of volcanic ash samples

We used two different volcanic ashes with contrasting properties to 'dose' the coupons.

For the 'salty' ash we were able to use a pristine ash sample collected in Nuku'alofa by a staff member of Tonga Geological Services following the 15 January 2022 eruption of Hunga volcano, Tonga. This ash serves as an analogue for ash from a future submarine eruption, for instance in the Auckland Volcanic Field.

For the 'acidic' ash, typical of ash generated by eruptions from Aotearoa's cone volcanoes, insufficient quantities of ash from recent eruptions of Ruapehu (1995-1996 eruptions) and Tongariro (2012 eruptions) volcanoes were available for experimentation. Therefore, we made an artificial sample using fine lahar deposits collected from the Whangaehu stream together with a sample of Whangaehu stream water. The lahar deposit samples were dried, homogenized, and sieved to <2 mm. Two different dosing solutions were prepared: unmodified stream water (pH 3.6) and stream water acidified to pH 1.4 with 10% sulphuric acid. Samples of lahar deposit were dosed with combinations of these solutions, dried, and then leachate solutions prepared using a 1:25 ratio of g ash to mL deionised water to test their surface composition. The 'acidic ash' sample chosen for the experiment had the properties described in Table 2.

The two ash samples were distinct with respect to their key characteristics of acidity and conductivity (a measure of ‘saltiness’).

Table 2 Properties of 1:25 leachate solutions of ash used for dosing

Property	Salty ash	Acidic ash
pH	6.2	3.6
Conductivity	2100 µS/cm	73.5 µS/cm

Building materials tested

Five types of metallic building material were tested in this study (Figure 2, Table 3). They are carbon steel, pure copper, hot-dipped galvanised zinc coating, 55wt.%Al-Zn alloy coating, and quartz-zinc (a titanium-alloyed zinc material).

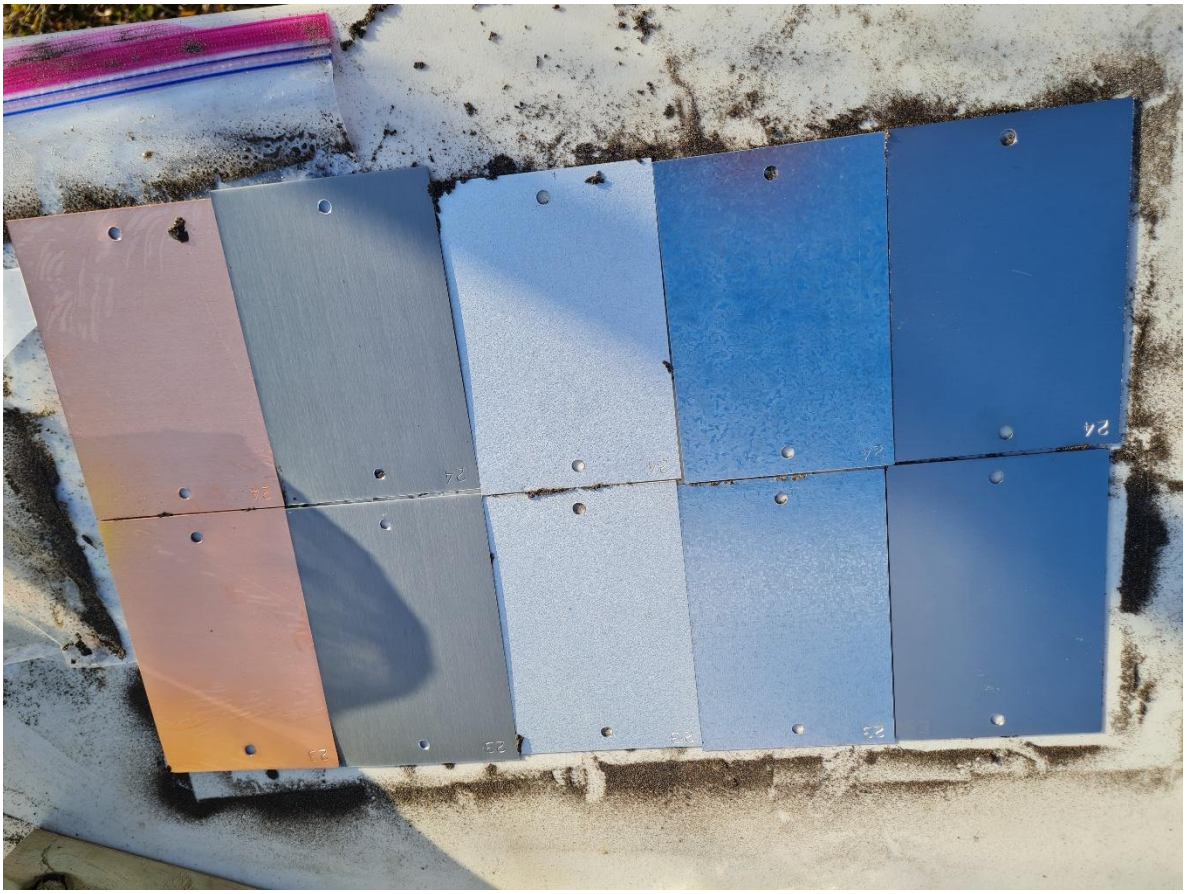

Figure 2 Metallic building materials tested in this study. From left to right: copper, quartz-zinc, aluminium-zinc alloy coating, HDG zinc coating, and carbon steel.

Chemical compositions of carbon steel and pure copper are given in Table 4.

Table 3 Materials tested in this study

Material	Uses
Carbon steel	This material is commonly used for atmospheric corrosivity classification according to national and international standards. Its corrosion rate, particularly first-year corrosion rate, is widely used as the baseline standard to classify environmental corrosivity.
Copper	Copper is widely used in power distribution systems as well as architectural cladding and guttering. It does suffer accelerated atmospheric corrosion-related damage in some areas within the Bay of Plenty region, particularly in Rotorua. A previous BRANZ investigation (Li et al., 2018) revealed that copper had a much higher sensitivity to the attack by (extremely) low concentrations of sulphur-containing geothermal species such as H_2S when compared with mild steel and zinc.
HDG	Hot dipped galvanized (HDG) zinc coating is widely used to protect carbon steel from atmospheric corrosion. This tough, metallurgically bonded coating provides enhanced corrosion resistance, structural durability by acting as a physical barrier and also lending a sacrificial protection. HDG coating can be applied for protecting steel structures, building claddings, and fastening/fixing components.
Aluminium-zinc alloy coating	55wt.% Al-Zn alloy coating is widely in New Zealand for both residential and commercial buildings as roofing, flashing, wall cladding, guttering, downpipes, and fencing due to its high corrosion resistance in mild and moderate environments.
Quartz-zinc	Pure zinc was not used in this study. Rather, quartz-zinc (the commercial name for this premium titanium-alloyed zinc product) was used. This material been pre-weathered to have a matte light-grey surface that offers “self-healing” scratch resistance and delivers long lifespan. It is widely used in contemporary architecture for roofing, cladding, facades and rainwater systems due to its high durability and minimal maintenance.

Table 4 Chemical composition of metallic samples used in the present study (wt.%)

Material	**Element**							
Carbon steel	C	Al	Si	P	S	Ti	V	Nb
	0.08	0.039	0.02	0.016	0.024	<0.005	0.01	<0.0005
	Cr	Mn	Ni	Cu	Mo	B	Fe	
	0.02	0.60	0.02	0.01	<0.01	<0.0006	Bal.	
Copper	Sn	Pb	Zn	Fe	Ni	P	S	Si
	0.006	0.010	≤0.0005	≤0.001	0.003	0.029	0.001	≤0.002
	Mn	Cd	Cr	Cu				
	≤0.0005	≤0.0005	≤0.0005	Bal.				

All materials were cut into coupons (150 mm × 100 mm) for exposure testing. The coupons were numbered and the dimensions of each coupon were measured. Prior to exposure, they were cleaned with acetone, dried with hot air and weighed to 0.001 g. The coupons were then sealed in separate plastic bags and shipped to the field sites.

Field deployment

The field deployment was carried out on 16 July (WWTP site, Figure 3) and 17 July (airport site) 2024 by team members CS, ZL, and KT.

Figure 3 View of WWTP deployment site

Figure 4 Dosing coupons with ash in the field.

Coupons were laid out on a table and then dosed with ash (Figure 4). Due to the smooth surface of the coupons and the installation at 45 degrees from vertical, it was necessary to lightly wet the surface of each coupon with a fine mist dispersed from a spray bottle to ensure that the ash would adhere to the metal surfaces. A solution of deionised water acidified to pH 5.0 with 10% sulphuric acid, to simulate rainfall partly acidified by contact with volcanic plumes, was used for the mist. Ash was then dispersed over coupons by shaking through a sieve to a thickness of approximately 1 mm and then allowed to dry in place prior to installation on exposure racks.

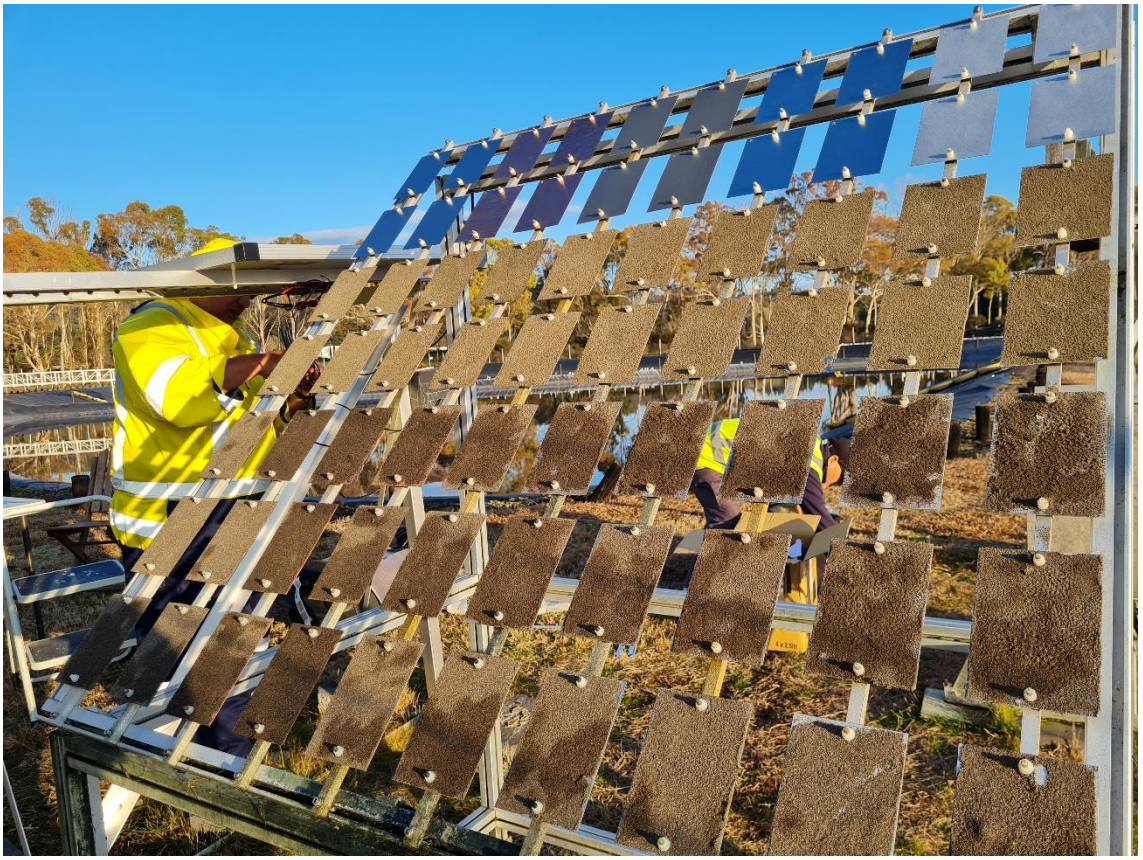

Figure 5 Coupons mounted on exposure rack. Top two rows of coupons are exposed to gas only; the lower rows are exposed to gas and ash.

Testing coupons were mounted onto purpose-built exposure racks that were fabricated with aluminium extrusions (Figure 5). Large separation distances were made between individual coupons to minimise potential cross-contamination and/or galvanic corrosion risk from corrosion products formed on carbon steel, copper, and zinc.

Nylon bolts, nuts, and washers were used to fix the metallic coupons onto the racks to avoid potential galvanic corrosion risks between testing materials and aluminium extrusions. Washers were also used to increase the gaps between the underside of the coupons and the aluminium supporting arms. This was to minimise water ponding and dirt accumulation in these sheltered areas and gaps.

The exposure racks were oriented towards north at an angle of 45° to the horizontal. In atmospheric corrosion testing, the 45° exposure angle is a standard method to evaluate how materials degrade outdoors. It provides a more consistent, standardised baseline for comparing different materials and corrosion rates derived from different locations. However, this angle is steeper than typical roof pitches used in New Zealand building practice, which generally range from 14° to 27°.

Analysis of coupons

After the designated exposure periods (~1 week, 1 month, 3 months, and 12 months), metallic coupons were retrieved for lab analysis. Each coupon was removed from its support and stored in a clean plastic bag for transport to the laboratory for analysis.

Their surface morphology was examined visually and microscopically.

Coupon cleaning procedure

The corrosion products remaining on the coupon surface were then cleaned thoroughly following the procedures recommended by ASTM G1 Standard practice for preparing, cleaning, and evaluating corrosion test specimens to determine corrosion rates.

- Carbon steel: 0.5 L/L hydrochloric acid (HCl, specific gravity = 1.19) + 3.5 g/L hexamethylenetetramine ($C_6H_{12}N_4$) at 20–25°C.
- HDG coating: 100 g/L ammonium chloride (NH_4Cl) at 70°C.
- Copper: 0.1 L/L sulphuric acid (H_2SO_4, specific gravity: 1.84, 98%) at 20–25°C.

The chemically cleaned coupons were rinsed with flowing water, dried with hot air and reweighed to determine their mass losses due to atmospheric exposure. Several clean, unexposed metal coupons were also immersed into these chemical solutions for the same period as the cleaning process. Their mass losses were recorded for corrosion rate measurement correction.

Please note that coupons of quartz zinc and Al-Zn alloy coating were not cleaned to remove corrosion products formed during atmospheric exposures in the present study.

Preparation of coupons for SEM analysis

Selected coupons were cut into samples of ~15 × 15 mm for characterisations using scanning electron microscopy (SEM) and energy-dispersive X-ray spectroscopy (EDS) (SU3800). Specifically, for surface morphological characterisation, samples were placed onto a specialised holder and coated with thin carbon film. For cross-sectional characterisation, samples were embedded into epoxy resin, ground, and polished down to 6 µm.

Meteorological variables

Weather conditions were monitored with a research grade weather station (Onset HOBO RX2102 Micro Station) deployed at the Rotorua airport site. This included ambient temperature, relative humidity (RH), dew point, wind speed, gust speed, wind direction, solar radiation, and rain. These climatic data were collected at 15-minute intervals.

Gas monitoring

An Airly air quality sensor (Figure 6a) was installed at the WWTP site on 16 July 2024. This sensor monitors airborne particulate matter (PM_1, $PM_{2.5}$ and PM_{10}), SO_2, H_2S, temperature, relative humidity, pressure and wind speed and direction. As the site had no access to mains power, power was supplied by a solar array (Figure 6b) using a 12 V 80 W solar panel and 12 V 9 Ah battery, which we replaced firstly with a 12 V 12 Ah battery and then with a 12 V 100 Ah battery after repeated problems. In total the sensor operated for 303 days over the year-long deployment period. Data was sent over the mobile network to Airly's data platform (Figure 7) from where we downloaded it.

Figure 6 Air quality sensor installed at wastewater treatment plant site. (a) Airly sensor and (b) solar array.

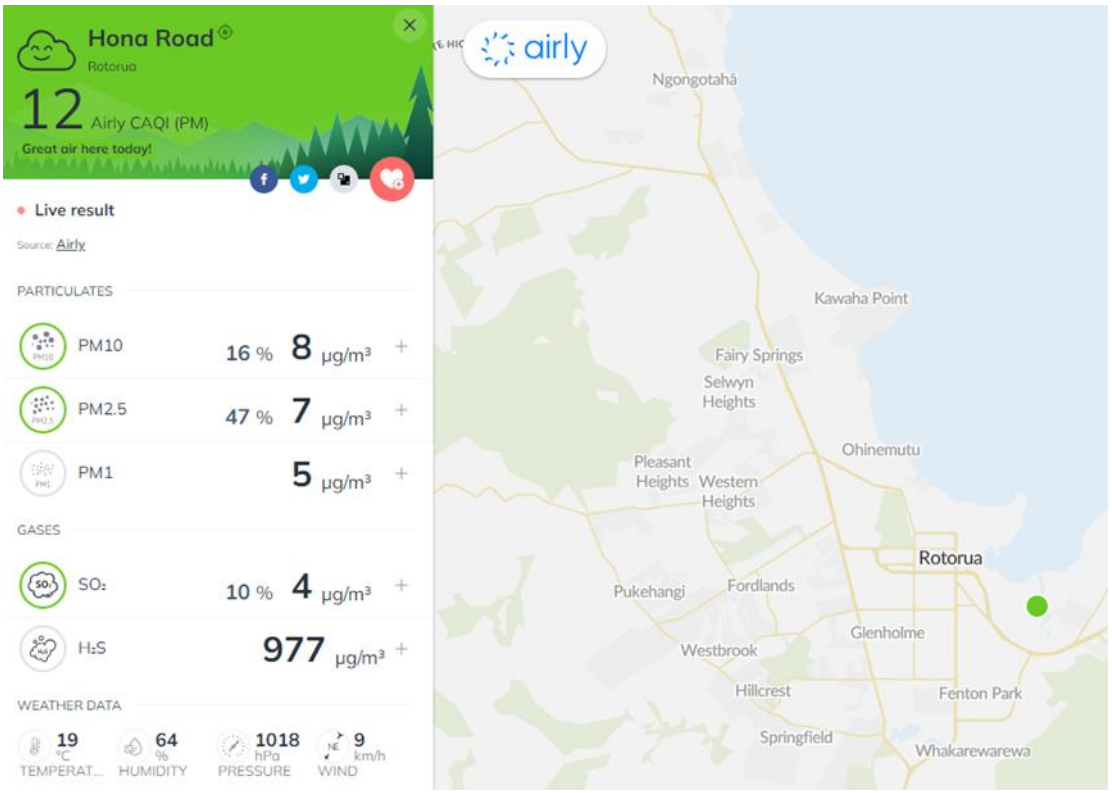

Figure 7 Example of real-time data displayed on Airly data platform

Spot measurements were obtained for H_2S and SO_2 during field visits using a handheld Aeroqual Series 500 meter. This instrument uses electrochemical gas-sensitive electrode heads.

We also deployed Gradko passive diffusion tubes on 16 and 17 July 2024 at both sites, for H_2S and SO_2. These were retrieved after three weeks and returned to the manufacturer in the United Kingdom for analysis. We did not continue with this method due to logistical difficulties of shipping, deploying, retrieving and return-shipping the tubes to the UK within a time window of a few weeks. See Appendix 1 for discussion of air quality data.

Results and discussion

Weather conditions

The highest ambient temperature was 30.3°C while the lowest was -2.5°C according to the weather station deployed at the Rotorua airport site during the 1-year monitoring period (July 2024 – July 2025). Relative humidity (RH) ranged from 28% to 100%, with a yearly average of 84%. The prevailing winds were from the north (N), southwest (SW), and west (W) (Figure 8). The maximum wind speed was approximately 7.5 m/s during this period.

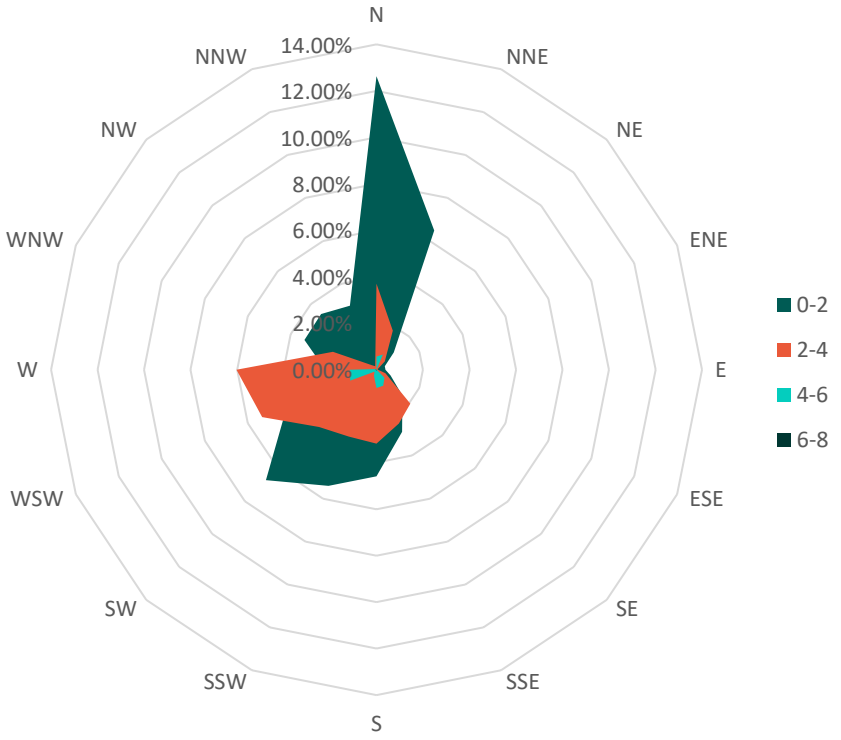

Figure 8 Wind speed and direct during the 1-year exposure period.

Rain is a critical factor in atmospheric corrosion. The rainfall following different exposure periods is presented in Table 5 for both sites. As expected, the two sites exhibit very similar rainfall patterns and total amounts.

Table 5 Rainfall (mm)

Exposure site	Exposure period			
	~1 week	1 month	3 months	1 year
Wastewater treatment plant	40	93.2	328	1359.4
Rotorua airport	40	93.2	328	1360

The total rainfall during the first week of exposure was the same at both sites, 40 mm. As a result, most volcanic ash was washed away from the coupon surfaces within the first two days of exposure. See Table 6 for detailed information on the rainfall events during the first week of exposure. Field exposure commenced on 16 July 2024 at the wastewater treatment plant site, and on 17 July 2024 at the Rotorua Airport site. There were significant rainfall events between 09:45 on 19 July and 14:15 on 20 July, with a total accumulation of 30.6 mm.

Table 6 Rain events in the first week of exposure. Events were of short duration (15 minutes or less) unless otherwise indicated.

Event	Date	Time of onset	Stop time	Rainfall (mm)
1	17/07/2024	17:45	20:30, 17/07/2024	1.4
2	17/07/2024	22:15		0.2
3	18/07/2024	03:15		0.2
4	19/07/2024	09:45	14:15, 20/07/2024	30.6
5	21/07/2024	13:30	16:00, 21/07/2024	3.6
6	21/07/2024	23:00		1.6
7	22/07/2024	00:15		0.2
8	22/07/2024	04:30	05:15, 22/07/2024	2
9	22/07/2024	08:45		0.2

After the first two weeks, volcanic ash could not be observed visually, particularly on coupons of hot-dipped galvanised zinc coating, Al-Zn alloy coating, and quartz zinc. These coupons have a relatively smooth surface. With a relatively large installation angle of 45°, the volcanic ash particles do not remain for long with rain washing.

Gas concentrations

Summary data for gas concentrations is presented in Table 7. Data for the wastewater treatment plant site was obtained using the Airly sensor and data for the airport obtained using a handheld Aeroqual monitor. The H_2S concentrations measured in this study are consistent with those reported by other studies, summarised by Hinz (2011). A monitoring campaign carried out by Environment Bay of Plenty (EBOP) at Ti St, central Rotorua, over the period 1998-2005, reported H_2S concentrations ranging from ~50-250 µg/m^3. The data showed a distinct diurnal pattern with higher concentrations during the night, and a seasonal pattern, with higher concentrations in autumn and winter (Iremonger, 2004; 2008). Siegel et al. (1986) recorded concentrations of 1700-5500 µg/m^3 H_2S on the southern

shores of Sulphur Bay at sites 450-700 metres from the wastewater treatment plant site. In this study, we recorded an hourly maximum concentration of 2370 µg/m^3.

Table 7 Summary statistics for H_2S concentrations data over deployment period

Gas	Measurement	WWTP	Airport
H_2S	Number of data points	303 daily averages	25 5-minute runs
	Maximum (µg/m^3)	1290	<5
	Mean (µg/m^3)	392	<5
	Median (µg/m^3)	324	<5
SO_2	Number of data points	*See appendix 1*	25 5-minute runs
	Maximum (µg/m^3)	-	<5
	Mean (µg/m^3)	-	<5
	Median (µg/m^3)	-	<5

Relationships between H_2S daily average concentrations and meteorological variables were investigated. Of these, only a relationship between H_2S and wind direction was observed, with the highest concentrations associated with winds from the northerly quarter (Figure 9). This is consistent with the location of the Sulfur Bay geothermal area to the north of the study site.

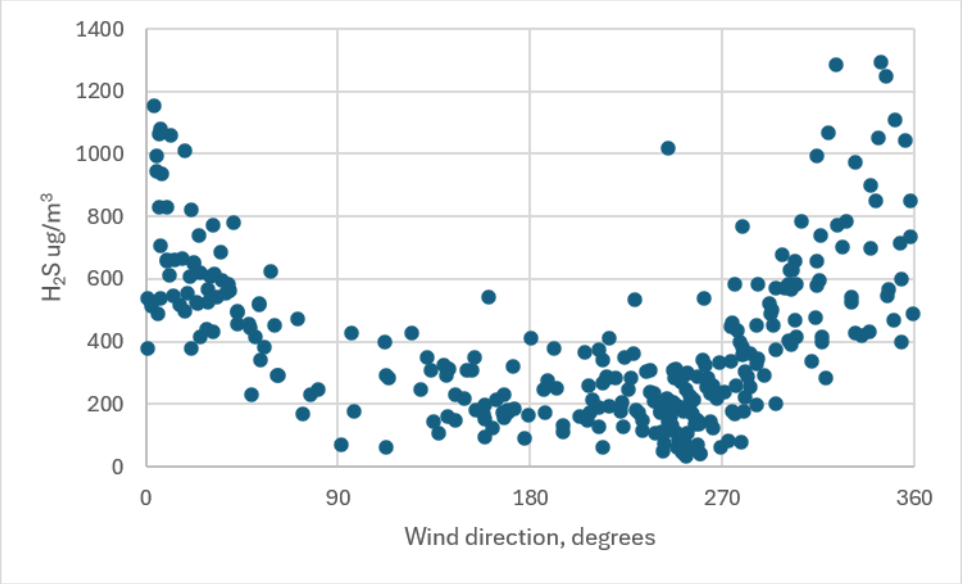

Figure 9 Daily average H_2S concentrations vs wind direction at WWTP site

No seasonal trends were evident in H_2S concentrations over the deployment period (Figure 10) in contrast to the EBOP monitoring dataset. This may be because the WWTP site is more strongly influenced by its proximity to Sulfur Bay than the site at Ti St.

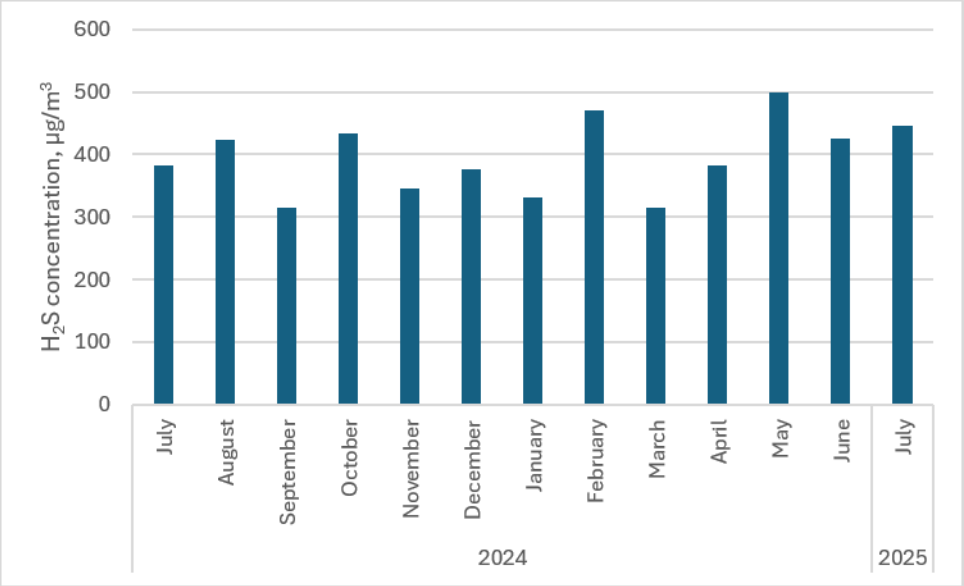

Figure 10 Monthly average H_2S concentrations over deployment period at WWTP site

Neither H_2S nor SO_2 were detected during field visits to the airport site.

We have chosen not to report on SO_2 data for the WWTP site because we became aware of a problem with false positive results for SO_2 in the presence of high concentrations of H_2S using electrochemical sensor methods. We discuss this further in Appendix 1. Henceforth, references to 'gas' mean hydrogen sulfide with an unknown but likely small amount of sulfur dioxide.

Time-dependent corrosion behaviour

Corrosion rates of carbon steel, copper, and hot-dipped galvanised zinc coating for coupons retrieved at one week, one month, three months and 12 months post-deployment are presented in Table 8.

Table 8 Summary of corrosion rate data

Material	Time	Corrosion rate (g/m²/year)						Corrosion rates from other BRANZ studies (g/m²/year)	
		Gas only		Salty ash		Acidic ash			
		WWTP	Airport	WWTP	Airport	WWTP	Airport	WWTP	Airport
Carbon steel	1 week	1,207	-	3,936	1,757	2,941	928	-	-
	1 month	1,496	-	3,794	880	3,425	686	2,251	487
	3 months	1,935	-	4,114	429	3,857	400	2,119	305
	12 months	3,303	-	3,547	272	3,386	242	1,888	199
Copper	1 week	855	-	642	191	777	190	-	-
	1 month	785	-	775	132	754	138	1,015	85

Material	Time	Corrosion rate (g/m²/year)						Corrosion rates from other BRANZ studies (g/m²/year)	
		Gas only		Salty ash		Acidic ash			
		WWTP	Airport	WWTP	Airport	WWTP	Airport	WWTP	Airport
	3 months	627	-	478	75	546	72	685	49
	12 months	273	-	239	40	267	46	481	33
Hot-dipped galvanized zinc coating (HDG)	1 week	108	-	188	199	241	134	-	-
	1 month	124	-	114	37	111	34	128 (Zinc)	10 (Zinc)
	3 months	92	-	91	37	84	32	88 (Zinc)	7 (Zinc)
	12 months	119	-	128	9	122	5	90 (Zinc)	4 (Zinc)

Results are discussed together with other experimental observations for each material in the following sections.

Carbon steel

Corrosion rate

Corrosion rates of carbon steel coupons for different exposure conditions at times of 1 week, 1 month, 3 months and one year are shown in Figure 11. Initial corrosion rates were highest for the exposure conditions of gas plus ash (with salty ash being higher than acid ash). Lower initial rates were recorded for salty ash only, gas only and then acid ash only.

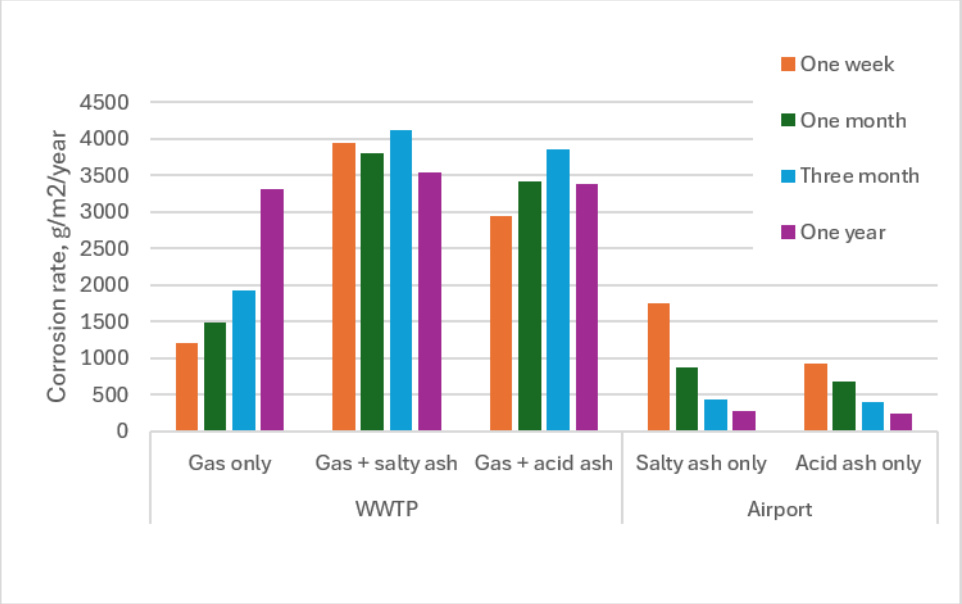

Figure 11 Corrosion rates of carbon steel for different exposure conditions at times of one week, one month, three months and one year

Surface morphology

Under all exposure conditions, the onset of corrosion was rapid, characterised by the formation of thick, iron-rich rust layers (Figures 12 and 13) after just one week's exposure.

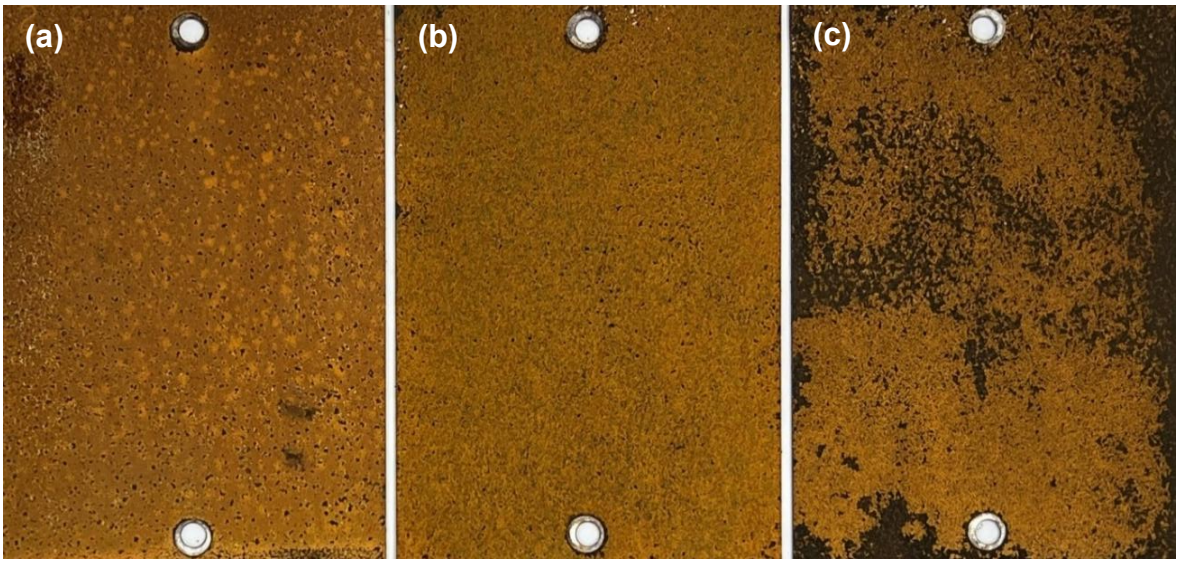

Figure 12 Surface morphology of carbon steel after one week of exposure at the WWTP site: (a) gas only, (b) gas plus salty ash, and (c) gas plus acidic ash.

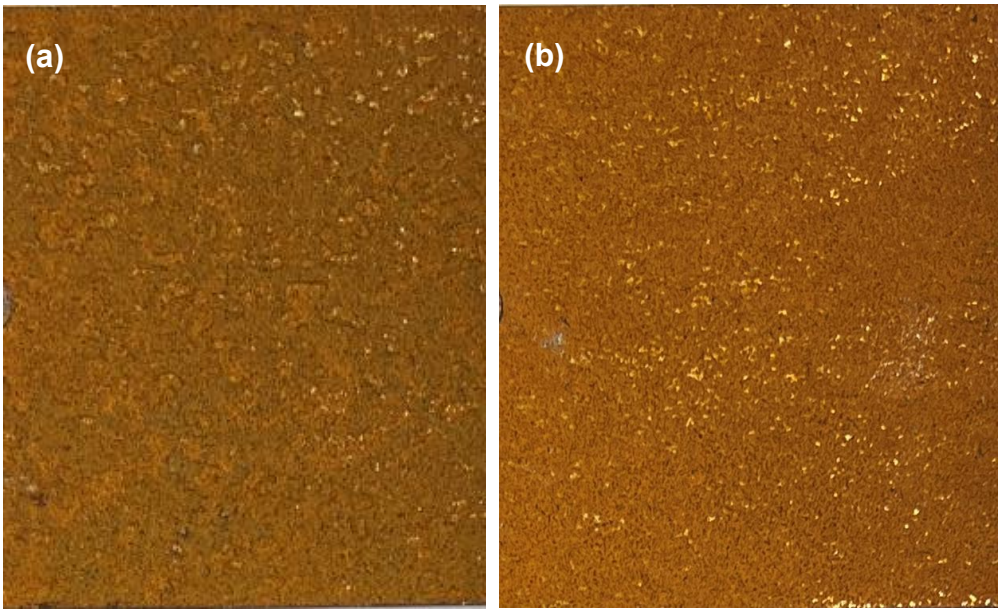

Figure 13 Surface morphology of carbon steel after one week of exposure at the airport site: a) salty ash only, b) acid ash only.

SEM and EDS analyses

SEM and EDS were used to collect morphological and compositional data to help understand corrosion processes and rates.

Exposure to gas only

Following one week's exposure to gas only, a thin layer of corrosion product, approximately 5-15 µm thick, was visible on the carbon steel coupon surface (Figure 14b). While it appeared to be largely continuous, cracks were visible on the surface (Figure 14a). These corrosion products are known to be iron oxides and oxide-hydroxides with sulphur contamination (Li et al., 2018).

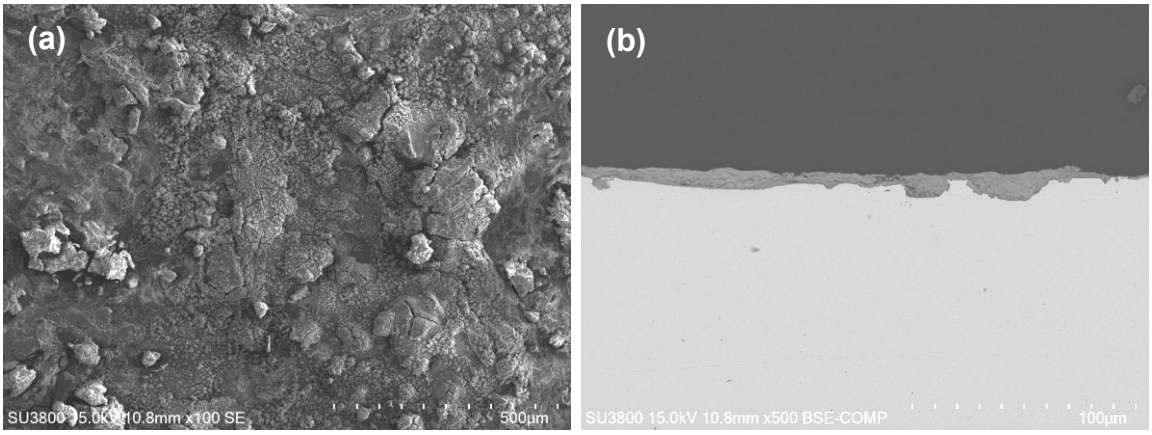

Figure 14 SEM characterisations of carbon steel exposed to gas only for 1 week: (a) top surface and (b) polished cross section.

After one month's exposure, the corrosion product layer had increased to approximately 20-60 µm thick (Figure 15b). Many cracks can be observed in the top surface (Figure 15a), and some long horizontal cracks are visible in the corrosion product layer and at the interface with the steel surface (Figure 15b). These cracks allow the ingress of gas which will react with the steel to form more corrosion products.

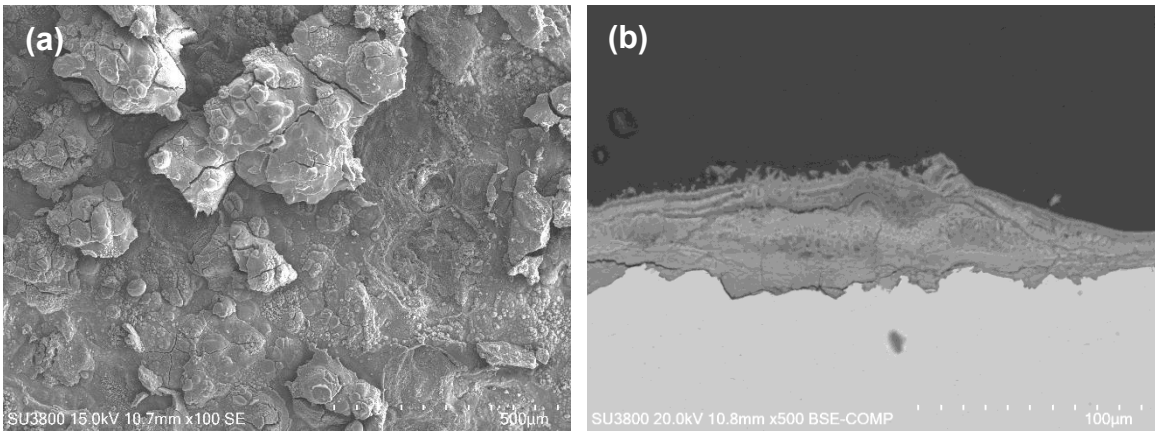

Figure 15 SEM characterisations of carbon steel exposed to gas only for one month: (a) top surface and (b) polished cross section.

With extended exposure, the corrosion rate continued to increase (Figure 11), and after a year the corrosion rate was almost three times greater than the one-week rate. This indicates that these corrosion products were non-protective and that their presence

might help retain corrosive agents from the surrounding environment to accelerate corrosion.

Exposure to gas plus ash

Volcanic ash particles were observed on the corroding carbon steel surfaces after one week's exposure (Figure 16). Although most ash particles appear to have been rapidly removed by rainfall, the loosely adherent, fast-growing iron-rich corrosion products retained some ash particles (in yellow circles) on the coupon surface. These particles had a large size range from approximately 10 µm to approximately 300 µm. There were clearly signs of interactions between ash particles and growing corrosion products.

Energy-dispersive spectroscopy (EDS) analyses showed that these particles primarily consisted of oxides of silicon (Si), aluminium (Al), iron (Fe), calcium (Ca) and magnesium (Mg), with lesser amounts of sodium (Na), potassium (K) and titanium (Ti). A remnant salty ash particle is shown in Figure 17 and an acidic ash particle in Figure 19. These compositions are consistent with the typical reported bulk composition of andesitic to basaltic andesitic volcanic ash (Genareau et al., 2016).

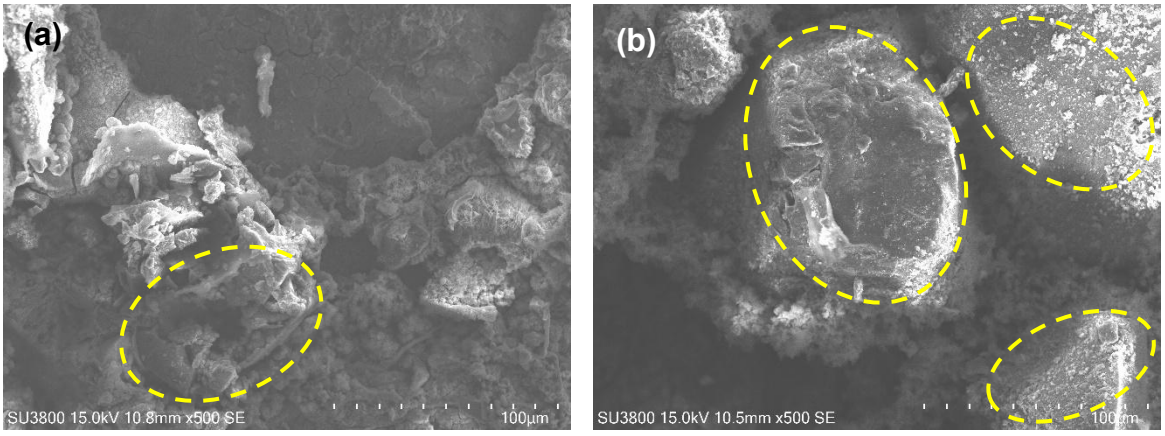

Figure 16 SEM surface morphology of carbon steel after 1 week of exposure: (a) salty ash and (b) acidic ash. Ash particles remaining on the surface are in yellow circles.

It is important to note that the EDS analyses provide information on the bulk composition of the adhered particles, and do not reflect the surface salts that were initially present on the ash samples used for doing the coupons, which have been removed by rainfall.

Gas plus salty ash

The cross section shown in Figure 18 shows that the corrosion product layer after one week for exposure to gas plus salty ash was more than 100 µm thick and was full of physical defects including pores and long horizontal cracks. Consistent with surface

observations (Figure 16a), ash particles were mainly contained towards the top of the layer of corrosion products although some smaller particles were partially embedded in the fast-growing layer of iron-rich corrosion products. Breakdown of ash particles could be observed.

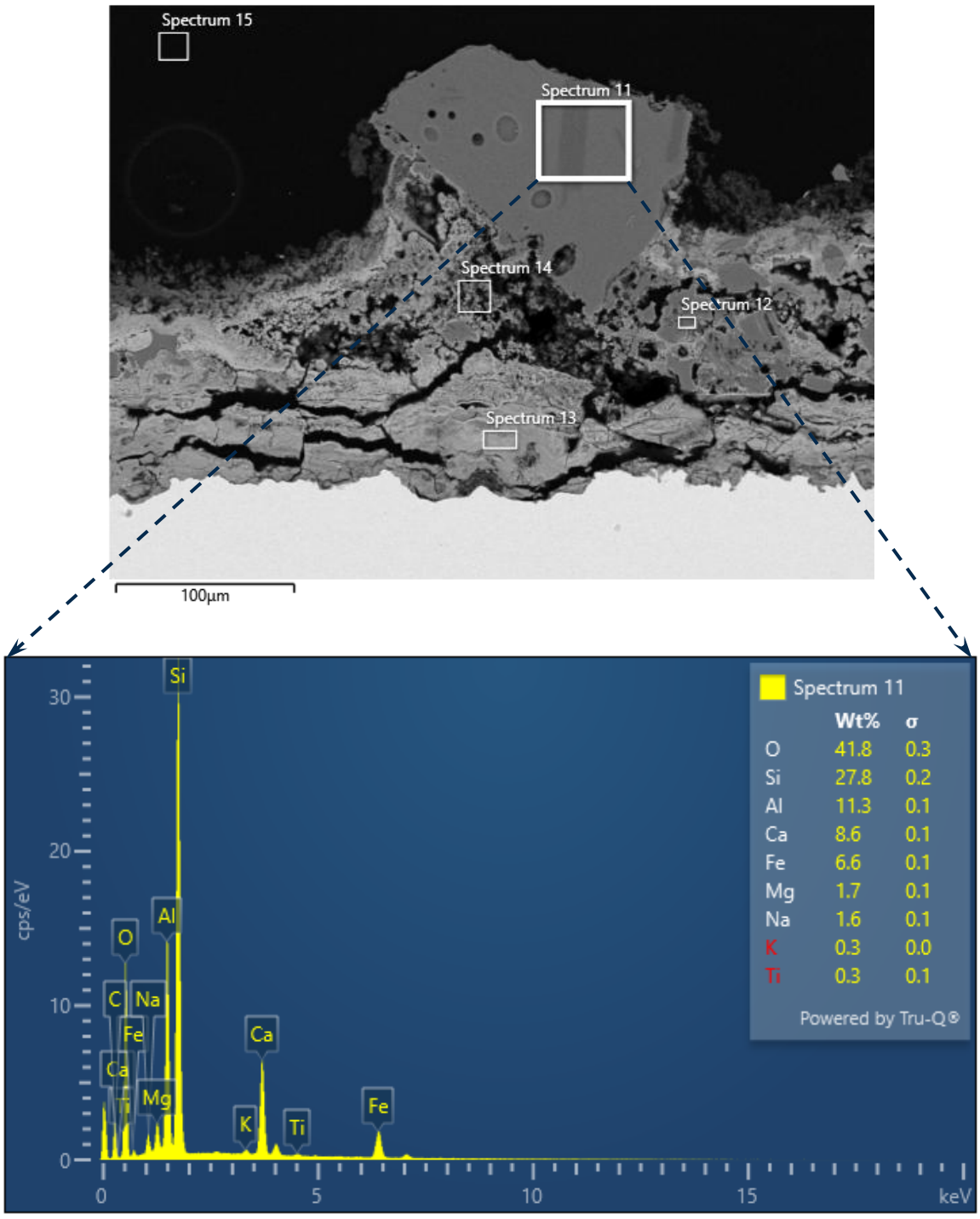

Figure 17 Energy dispersive X-ray spectroscopy (EDS) analysis of the elemental composition of a large salty ash particle remaining on the carbon steel coupon after one week of exposure. SEM image was taken from the polished cross-section.

After one month's exposure, the layer of corrosion products appeared more consolidated but had deep fissures reaching to and along the metal surface (Figure 18). There were no remaining ash particles visible.

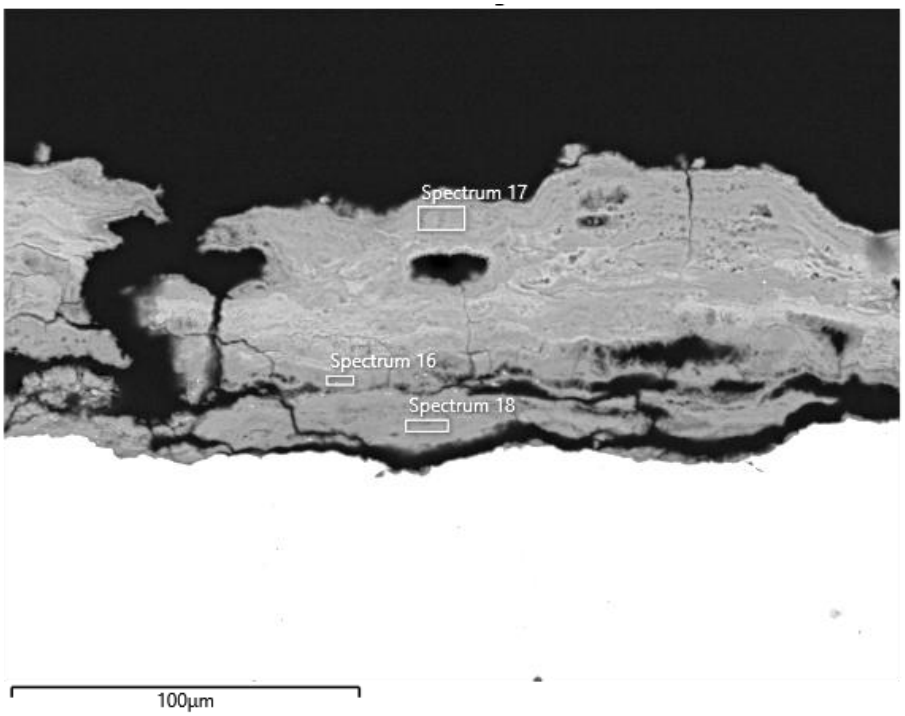

Figure 18 SEM image of polished cross section of carbon steel coupon exposed to gas plus salty ash for one month. Spectra 17-19 are all dominated by Fe and O with minor traces of S contamination.

Gas plus acidic ash

Figures 19 and 20 show elemental surface composition and elemental composition for a cross section for carbon steel coupons exposed to gas plus acidic ash for one week. As for the gas plus salty ash exposure, iron-rich corrosion products have grown rapidly outwards and penetrated into gaps between ash particles.

For carbon steel coupons exposed to gas plus acidic ash for one month (Figure 21), the particles 'trapped' in the layer of corrosion products (Figure 20) are no longer visible. A very thick layer of corrosion products (~ 260 µm thick) has formed. This layer has many physical defects including cracks and fissures that would allow gas to penetrate through to the metal surface as well as severe spallation. Ash particles may have been lost through (partial) spallation of corrosion product layers.

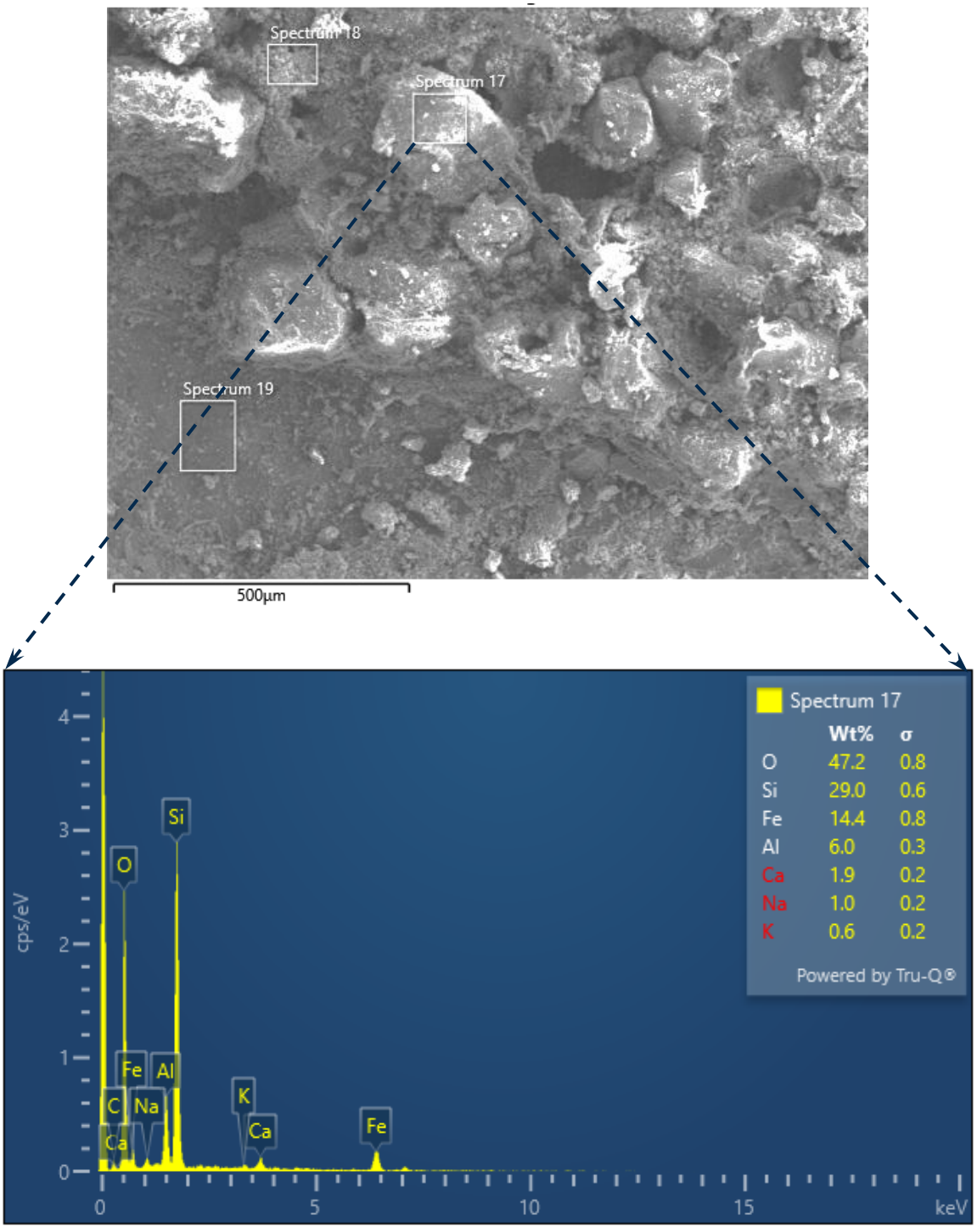

Figure 19 Energy dispersive X-ray spectroscopy (EDS) analysis of the elemental composition of an acidic ash particle remaining after one week of exposure. SEM image was taken from the top surface of the carbon steel coupon.

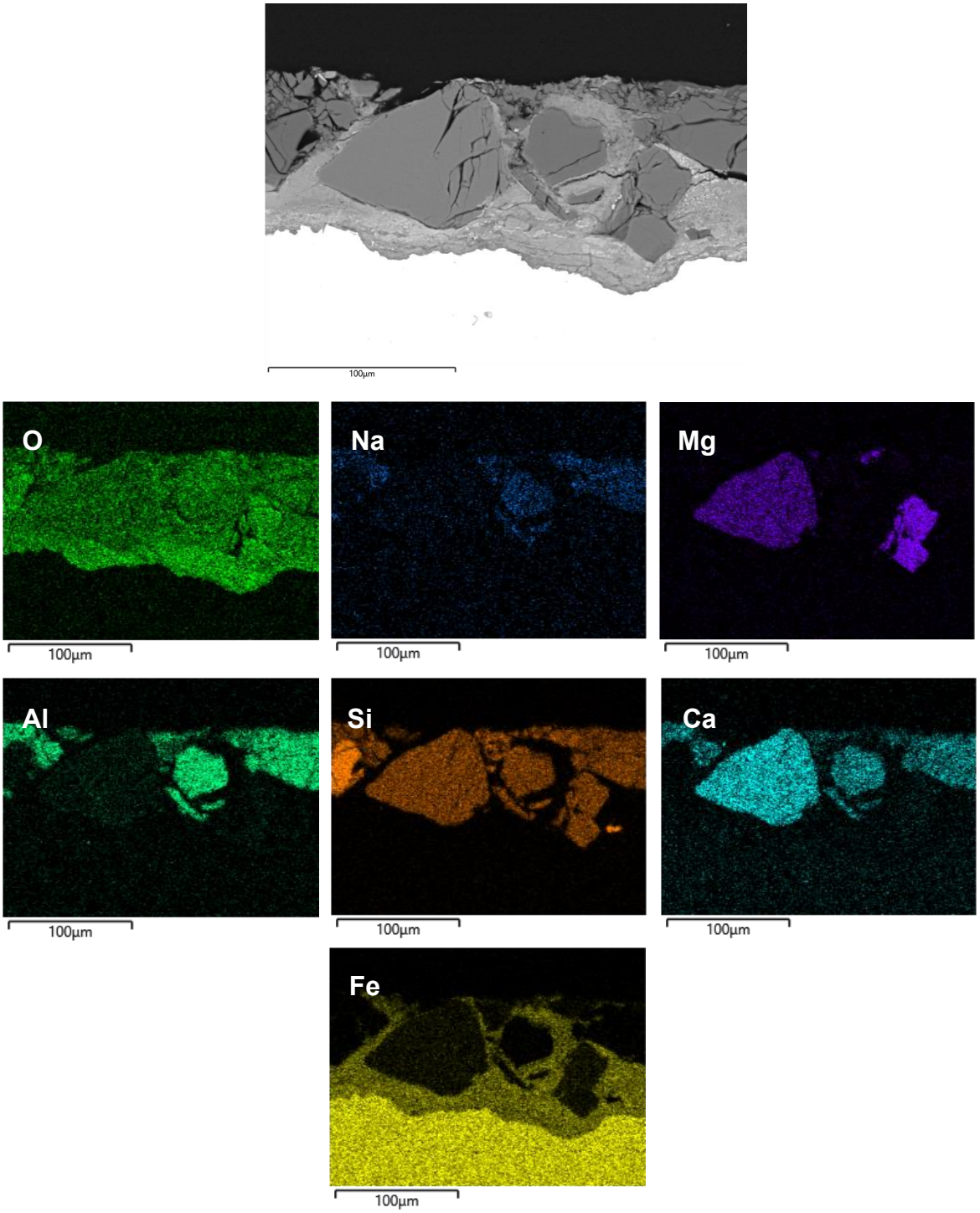

Figure 20 Energy dispersive X-ray spectroscopy (EDS) elemental mapping for coupon exposed to gas plus acidic ash after one week exposure. SEM image is for a polished cross section of the carbon steel coupon.

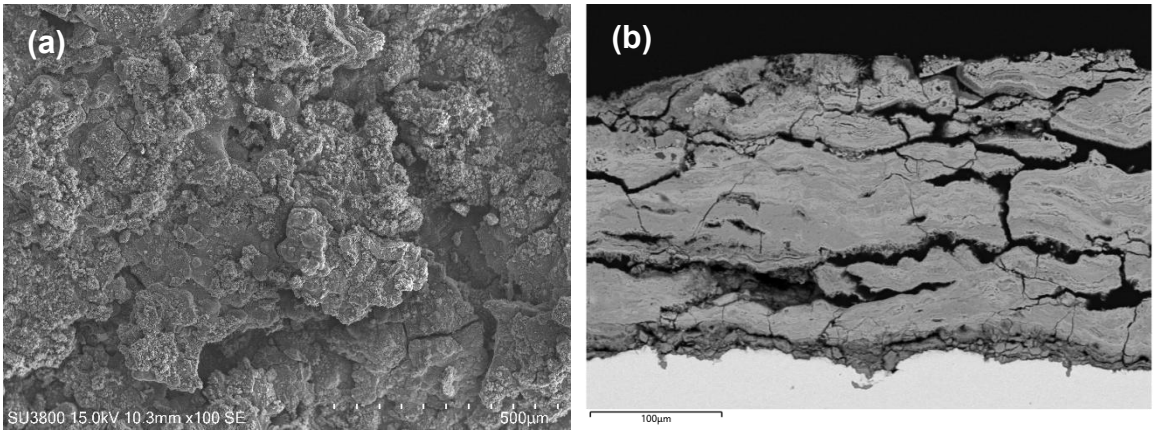

Figure 21 SEM characterisations of carbon steel coupons exposed for one month to gas plus acidic ash: (a) top surface and (b) polished cross section. The corrosion product layer is approximately 260 µm thick.

Exposure to ash only

Salty ash

One-week corrosion rates for coupons exposed to ash only were similar to those exposed to gas only, with the rate for salty ash approximately double that for acidic ash (Figure 11). A SEM cross section (Figure 22) shows that a layer of corrosion products up to ~50 µm thick has formed underneath the salty ash layer, which appears to be disintegrating.

After a month's exposure, there is further growth of corrosion products into the interstices between particles, and particles also appear to be breaking down (Figure 23). The initial corrosion may have been initiated by the surface salts (high in sodium chloride) present on the fresh ash, but once these salts have been leached by rainfall, the corrosion rate trends back towards its baseline rate in this environment (Table 8).

Acidic ash

For the carbon steel coupons exposed to acidic ash for a week, there was also rapid growth of a layer of corrosion products into the interstices between ash particles (Figure 24). The layer was somewhat thinner although many physical defects such as long horizontal cracks are visible. After a month (Figure 25), as for the salty ash, particles appear to be breaking down. Similarly, as for the salty ash, once the particles have been removed, the corrosion rate trends back towards its baseline.

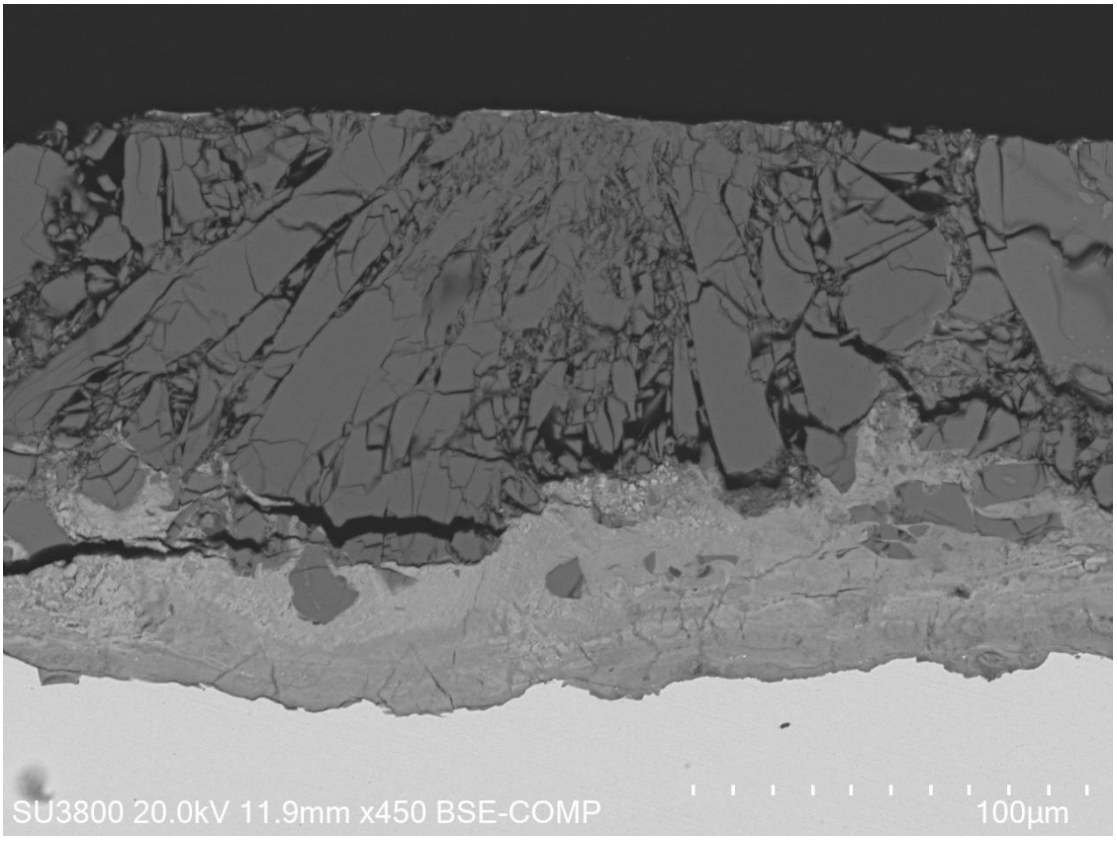

Figure 22 SEM characterisation of a polished cross section of a carbon steel coupon exposed to salty ash only for one week.

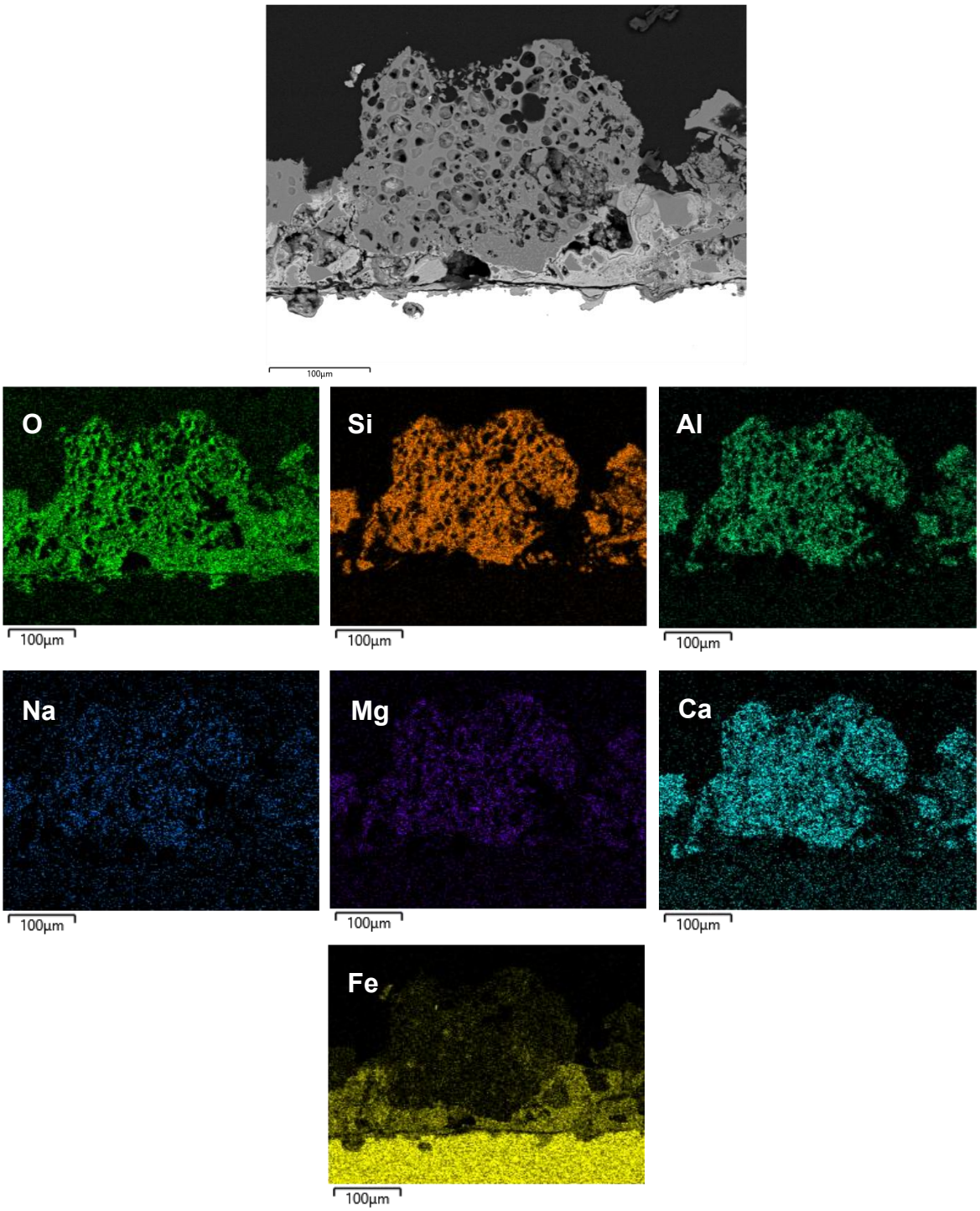

Figure 23 Energy dispersive X-ray spectroscopy (EDS) mapping of elemental composition of a polished cross section of a carbon steel coupon exposed to salty ash only for one month.

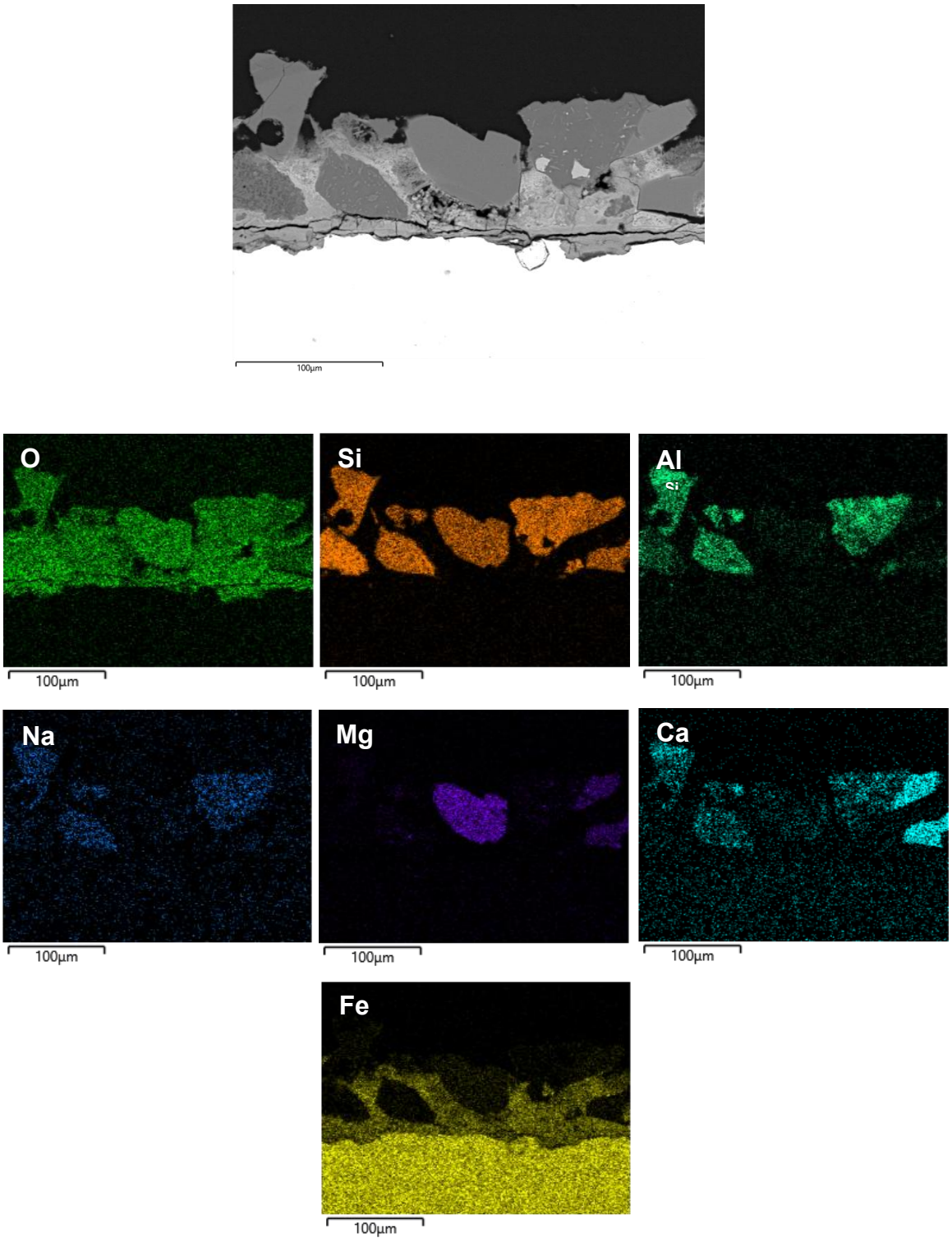

Figure 24 Energy dispersive X-ray spectroscopy (EDS) mapping of elemental composition of a polished cross section of a carbon steel coupon exposed to acidic ash only (Rotorua airport) for one week.

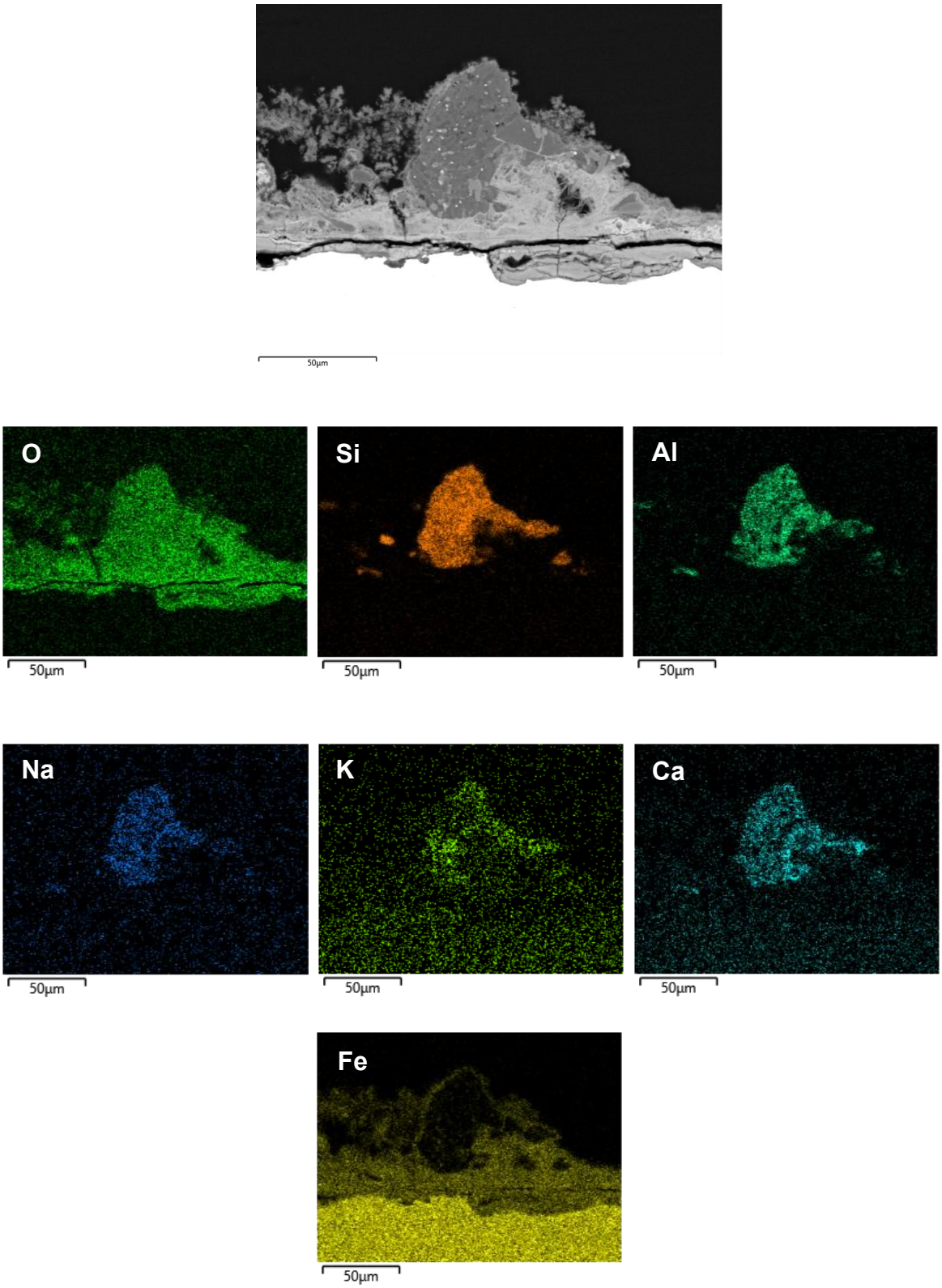

Figure 25 Energy dispersive X-ray spectroscopy (EDS) mapping of elemental composition of a polished cross section of a carbon steel coupon exposed to acidic ash only for one month.

Kinetics

Different corrosion kinetics over time were observed for the three different exposure situations (Figure 11). While there was rapid onset of corrosion for all exposures in the short term, differences emerged over the course of the year.

For the combined ash plus gas exposures, initial corrosion rates were 2-3 times higher than for the ash-only or gas-only exposures. This may be due to the rapid formation of corrosion products that grew outwards from the metal surface and enclosed the ash particles (Figures 17 and 20). These corrosion product layers were full of physical defects such as pores and cracks that would have allowed ingress of corrosive gas and/or moisture to the metal surface as well as being unstable and prone to removal by spalling. After a month, ash particles were no longer visible within the corrosion products, and the layers appeared more cohesive. The corrosion rate did not markedly increase through the year.

For the gas-only exposure, corrosion rates were initially lower than when ash was present. A thin but fairly uniform layer of corrosion products formed, then began to grow rapidly (Figures 14b and 15b). The corrosion rate continued to increase throughout the year, and by the end of the year it was comparable to the ash plus gas exposure. This indicates that the corrosion products formed were not protective and may have acted to trap moisture and gas from the surrounding environment. As the corrosion product layer thickened, a whole layer may have detached completely from the underlying substrate. This would have significantly reduce the corrosion products remaining on the surface, which could have acted as a barrier for further attack.

For the ash-only exposure, the initial corrosion rates were similar to those for the gas-only exposure. SEM analyses of cross sections showed that the ash layer was relatively intact after one week, with limited growth of corrosion products. However, after one month of exposure, the ash particles appeared to be disintegrating and corrosion products building up. The presence of the ash particles may have promoted corrosion by trapping moisture. Over the course of the year, the corrosion rate decreased steadily for both types of ash. The initial corrosion may have been initiated by the surface salts (high in sodium chloride), or acids, present on the fresh ash, but once these salts/acids have been leached and ash particles removed by rainfall, the corrosion rate trends back towards its baseline rate in this environment (Table 8).

Salty versus acidic ash

The two ash samples used for dosing coupons in the presence and absence of ash had contrasting properties in their fresh (unaffected by rainfall) state. The ‘salty’ ash had a high concentration of surface salts dominated by sodium chloride, and the ‘acidic’ ash formed an acidic leachate to mimic ash typical of that generated by Aotearoa’s cone volcanoes (Cronin et al., 2003, 2014).

For the combined ash and gas exposure, salty ash had a more rapid initial corrosion rate than acidic ash, but this difference reduced over time. After a week’s exposure, a thick but unstable corrosion layer full of physical defects formed (Figure 17). In contrast, for acidic ash the layer of corrosion products after a week’s exposure was thinner and more cohesive (Figure 20). These differences reduced after a month’s exposure.

For the ash-only exposure, salty ash also had a more rapid initial corrosion rate than acidic ash with the difference reducing as the year progressed. The most visible difference between SEM cross sections at one week exposure is the thicker layer of corrosions products underneath the ash layer for the salty ash. As for exposures with gases, differences reduced over time.

Overall, there was a rapid onset of corrosion under all exposure conditions, despite both sites receiving 40 mm rainfall over the first week.

The fastest initial corrosion rate was recorded for the combination of ash plus gas. This is thought to be due to the rapid growth of an unstable layer of corrosion products (iron-rich oxides and oxide-hydroxides) that trap ash particles and allow ingress of gas to the metal surface, increasing corrosive attack on the steel substrate. The trapped particles may also facilitate the retention of moisture.

The presence of volcanic ash alone, whether ‘acidic’ or ‘salty’, can accelerate corrosion. One-month, three-month, and one-year corrosion rates for ash exposure only were higher than those derived from other BRANZ studies carried out at the study location.

These findings support the advice to remove ash from steel components of buildings as soon as practicable and safe to minimise risk of corrosion developing. This is particularly the case if there is exposure to gas as well. But even in the absence of gas, the presence of ash is likely to accelerate corrosion.

Copper

Corrosion rates

A previous study (Li et al., 2018) found that copper is very sensitive to sulphur-containing gas emissions from geothermal sources. As a result, its corrosion rate could be very high, even in areas with low concentrations, for example, western regions of Rotorua city.

At the wastewater treatment plant site with high gas concentrations, rapid and severe corrosion was observed on copper coupons with and without surface volcanic ash coverage (Table 8, Figure 26).

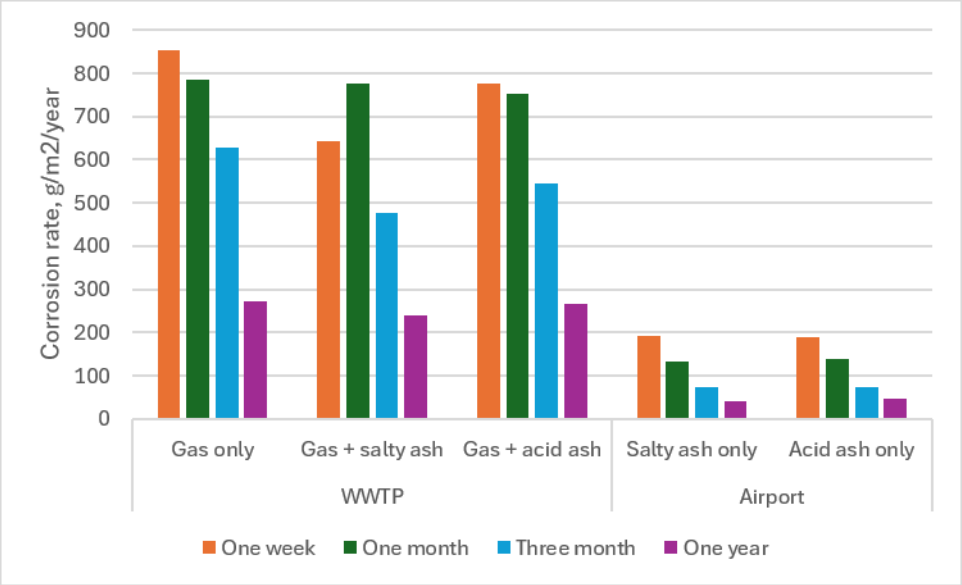

Figure 26 Corrosion rates of copper for different exposure conditions at times of one week, one month, three months and one year

However, the first-week corrosion rates of the coupons exposed to gas plus surface ash coverage were lower than those exposed to gas only. These differences were also apparent for the three-month exposure, but had reduced by the end of a year.

Comparing the one-week corrosion rates for exposures to gas only vs ash only, clearly gas is the more corrosive agent than ash.

Kinetic behaviour was similar across all exposure conditions, with decreasing corrosion rates over time. This suggests that the corrosion products formed were, to a large extent, protective. Copper exhibited relatively high corrosion rates; however, most of its corrosion products remained adherent to the surface, with only limited spallation occurring in localized, patchy areas. Consequently, these corrosion products could act as a physical barrier, reducing the interaction between corrosive gases and the underlying copper.

The copper coupons with ash only exposure displayed similar time-dependent corrosion kinetic behaviour, i.e. corrosion was slowing down with time.

SEM morphological and compositional analyses

Gas-only and gas plus ash exposures

SEM observations indicated that the top surface of the copper coupon exposed to gas only was covered with a reasonably uniform and dense layer of corrosion products (a mixture of copper oxide and sulphide) after one week of exposure (Figure 27a). In comparison, the top surfaces of the copper coupons exposed to gas plus ash were slightly rough, with the formation of many small-sized particles and disk/plate-like structures (Figures 27b, 27c).

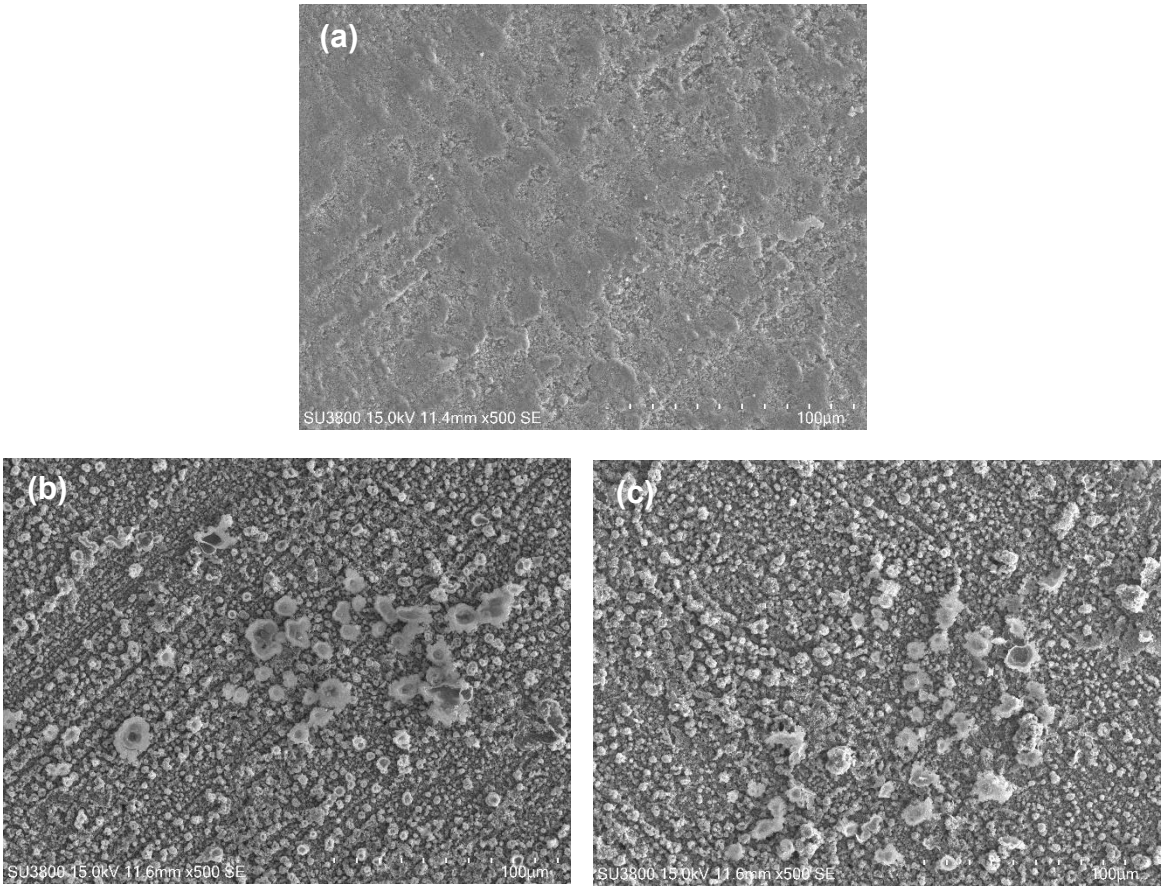

Figure 27. Surface morphology of copper coupons after 1 week of exposure at the wastewater treatment plant site. (a) gas only (b) gas plus salty ash, and (c) gas plus acidic ash.

EDS analyses indicated that those disk/plate structures were more sulphur-rich when compared with those smaller corrosion particles or clusters (Figure 28). Furthermore, the surface morphologies of the copper coupons covered with salty and acidic ash were very similar. Based on this morphological observation, it may be expected that ash coverage would accelerate corrosion, at least within the first week of exposure, as it did with carbon steel. However, this was not supported by corrosion rate measurements.

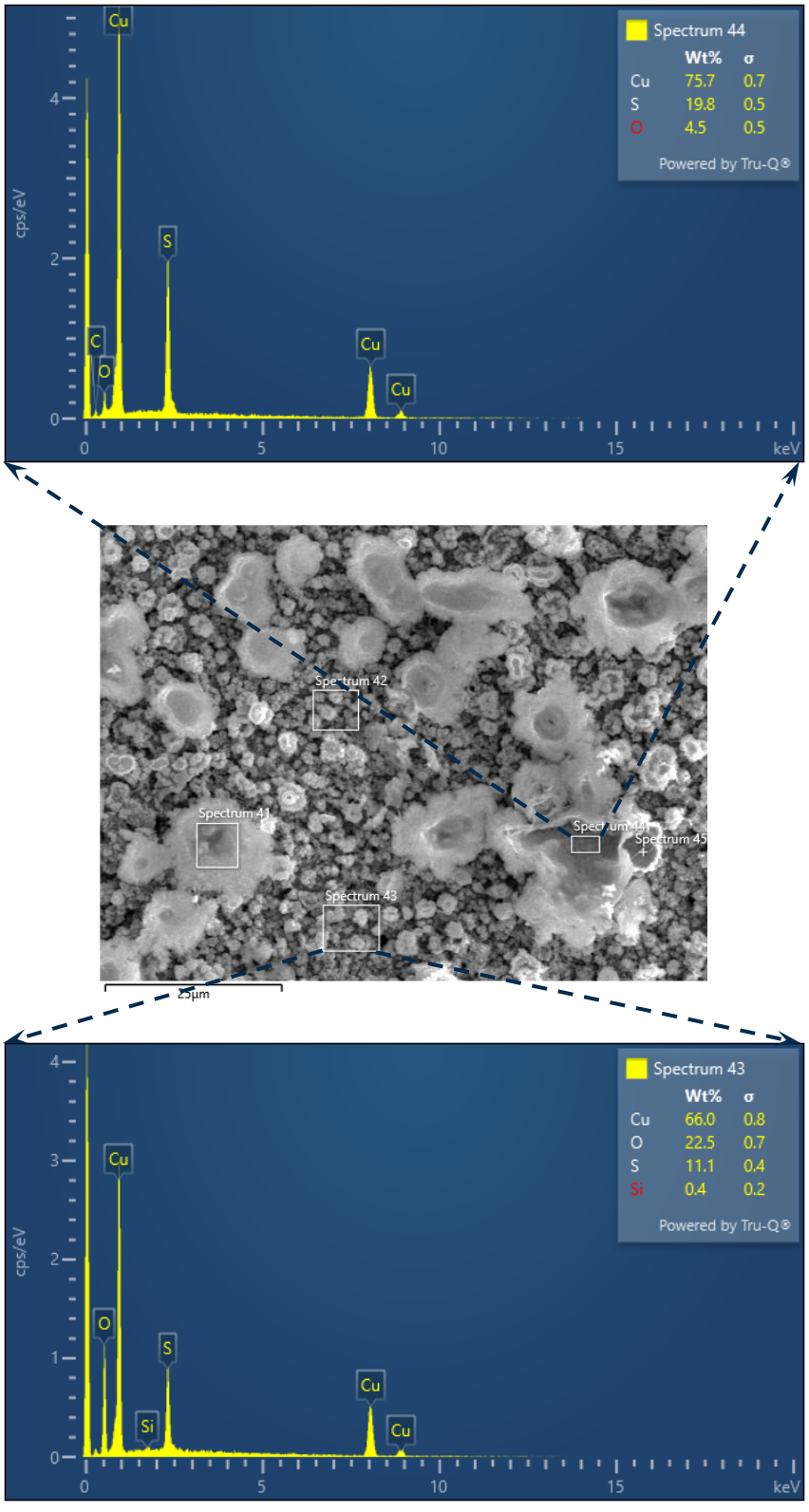

Figure 28 EDS compositional analyses of corrosion products on copper coupon after one week exposure to gas plus salty ash.

After a month's exposure, the surface morphologies of the coupons exposed to gas with and without ash coverage appear similar (Figure 29). As for the one-week exposures, no ash particles were visible on the surface.

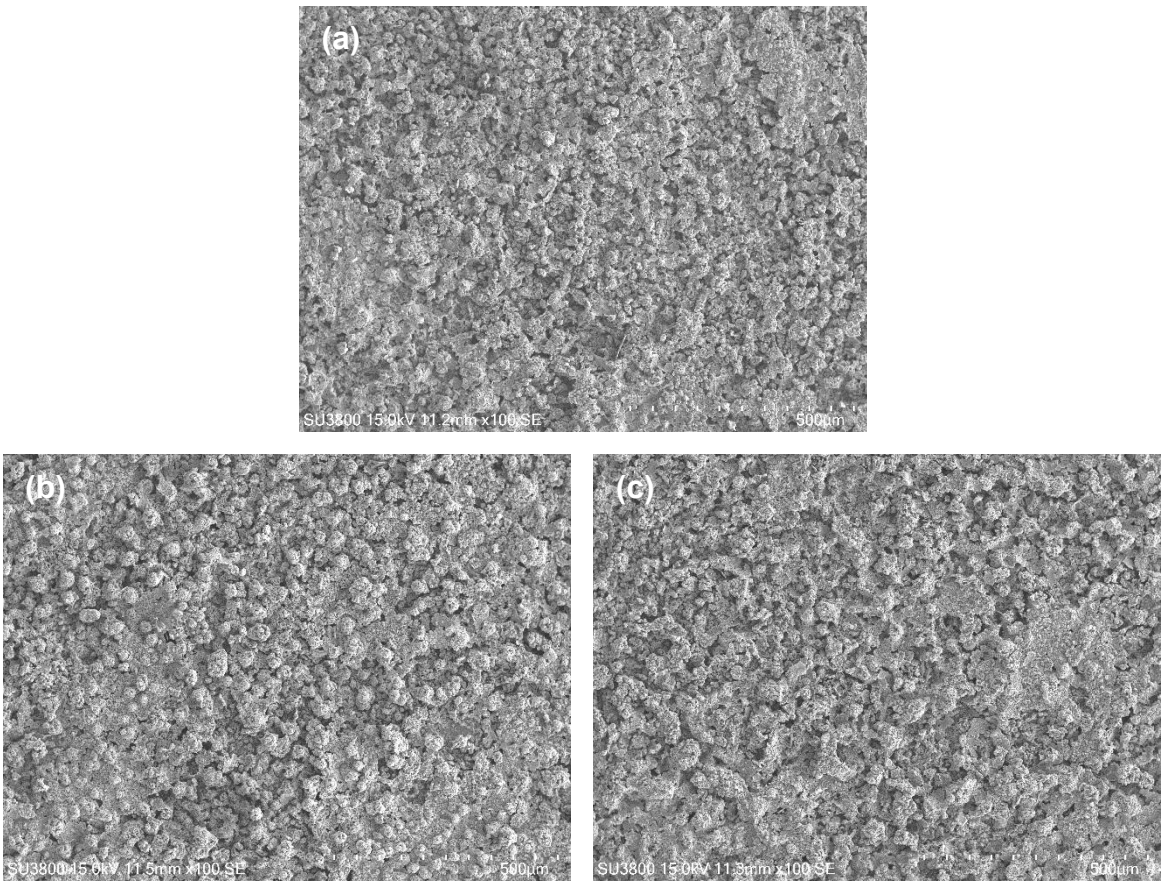

Figure 29 Surface morphology of copper coupons after one month of exposure to (a) gas only, (b) gas plus salty ash, and (c) gas plus acidic ash.

Copper is known to be extremely sensitive to sulphur-containing gases in the air (Li et al., 2018). Previous studies in the field with strong geothermal emissions found that freshly prepared copper surfaces can react with sulphur-containing gases in the air very quickly. Surface colour starts to change after a few minutes of exposure, indicating a very rapid interaction of copper with gas in the air in the absence of high moisture or rain.

From this perspective, the thin ash layer, approximately 1-2 mm thick, may have acted as a physical barrier to partly reduce the contact between copper and gas in the air. This might be particularly true in the first few days of exposure. In the later stage of the first week, ash particles were removed by rainwater, and all coupons were then exposed to the same atmospheric environment.

Ash-only exposures

For coupons exposed to ash alone, the corrosion products (a mixture of oxides and sulphides) were uniform and dense (Figure 30). They appear to be more protective compared with those that formed on coupons exposed to both ash and gas (Figure 27).

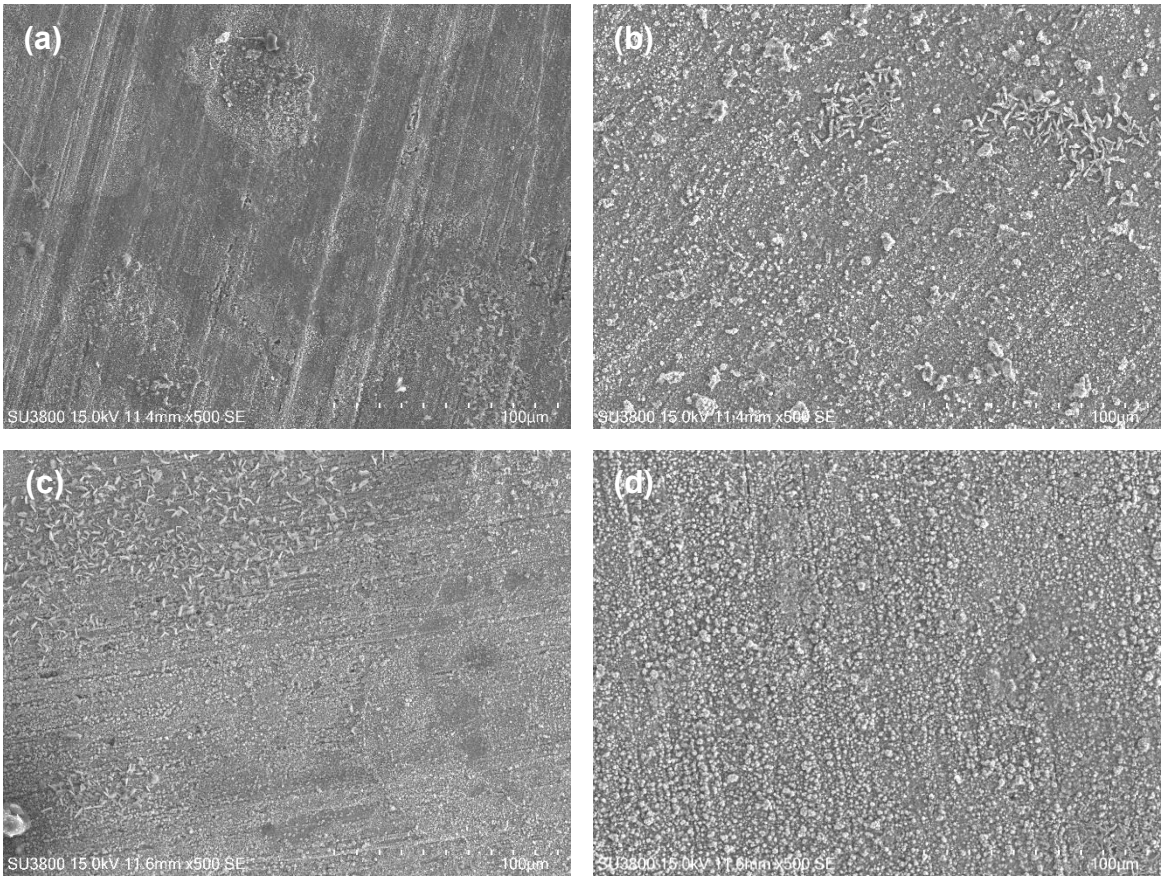

Figure 30 Surface morphology of copper coupons exposed to: (a) salty ash only for one week, (b) salty ash only for one month, (c) acidic ash only for one week, and (d) acidic ash only for one month.

While ash particles were not observed on metal surfaces after a week's exposure, an outline was visible in Figure 31a. EDS elemental analyses (Figure 31) revealed trace quantities of silicon, iron and aluminium, characteristic of ash particle bulk composition. This suggests interactions between the ash particles and the copper surface in the initial stages of exposure.

Overall, copper is much more susceptible to corrosive attack by volcanic gas than by volcanic ash. For coupons exposed to gas plus ash, the ash coverage may have provided initial protection by acting as a physical barrier between the metal and the gas. However, unlike carbon steel, copper has no ability to retain particles on its surface with corrosion products, thus this protection was short-lived. While ash is not strongly corrosive towards copper, corrosion was more rapid for coupons exposed to ash alone than for baseline measurements at the same study site, thus its removal is still recommended.

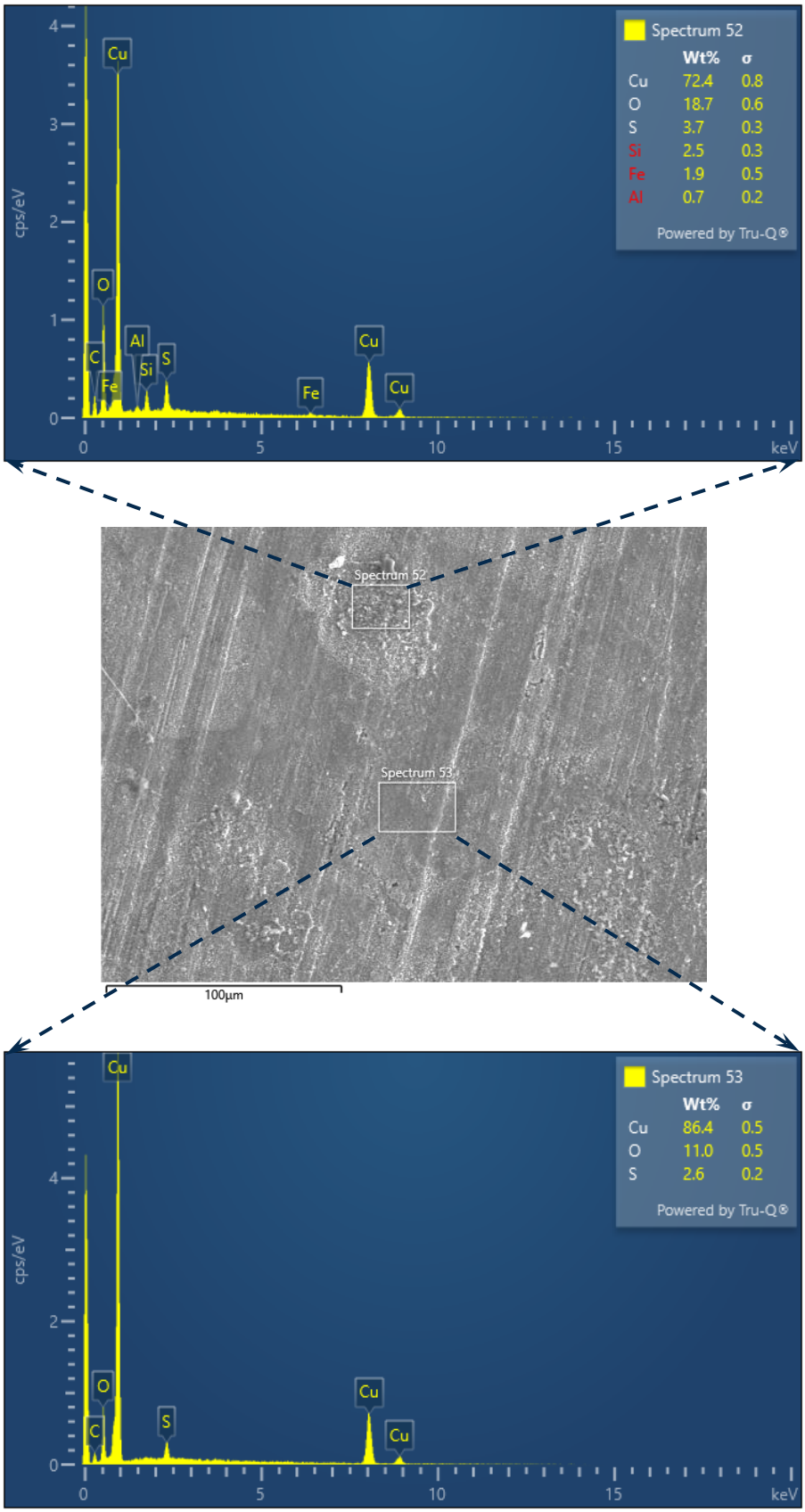

Figure 31 SEM-EDS compositional analyses of corrosion products remaining on copper coupons after one week of exposure to salty ash only

Hot dipped galvanized (HDG) zinc coating

Corrosion rates

For short exposures of one week, the presence of ash led to increased corrosion rates for coupons exposed to both gas plus ash and ash compared to gas only (Figure 32). However, for longer exposures, exposure to gas was more important. Initially there were differences between salty and acid ash, but these differences disappeared after the first week of exposure. For the sites exposed to gas, after the first week the corrosion rate remained steady over time, implying that the corrosion products formed were not protective, but for the site exposed to ash only, the corrosion rate had decreased markedly towards the baseline rate for this site (Table 8).

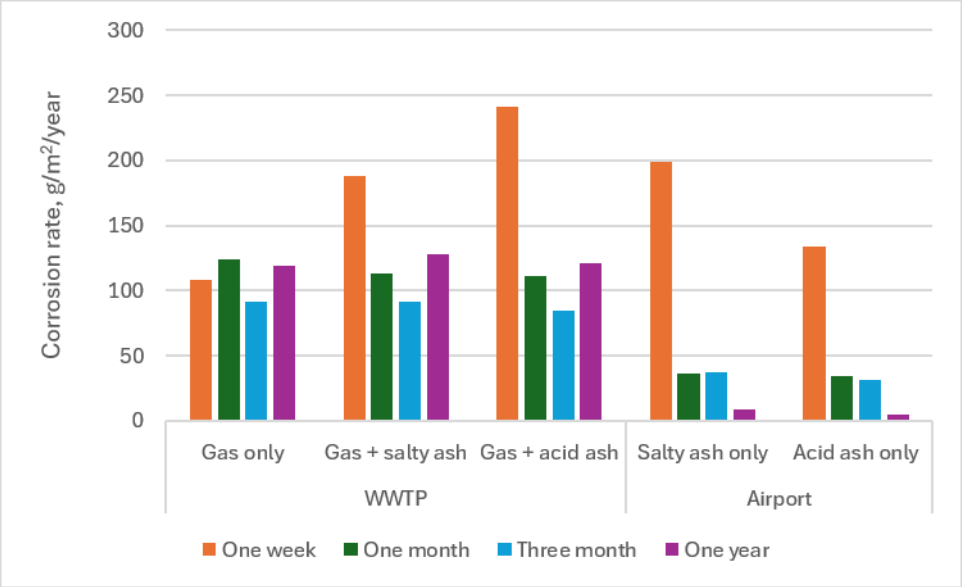

Figure 32 Corrosion rates of HDG for different exposure conditions at times of one week, one month, three months and one year

Morphological and compositional analyses

Exposures to gas only and gas plus ash

After a week's exposure, coupons exposed to gas only were similar to those exposed to gas plus ash or ash only (Figure 33) although some small surface features were found only on the coupons exposed to ash (Figure 33(c) and 33(e)). EDS compositional analysis (Figure 34) indicated that these features were rich in silicon, calcium, magnesium, and aluminium, suggesting that they are residuals of ash contacting with the metal surface. The more rapid rates of corrosion for the ash-covered panels could be explained by the presence of these features which increase the effective surface area, attracting more moisture and gas to accelerate corrosion.

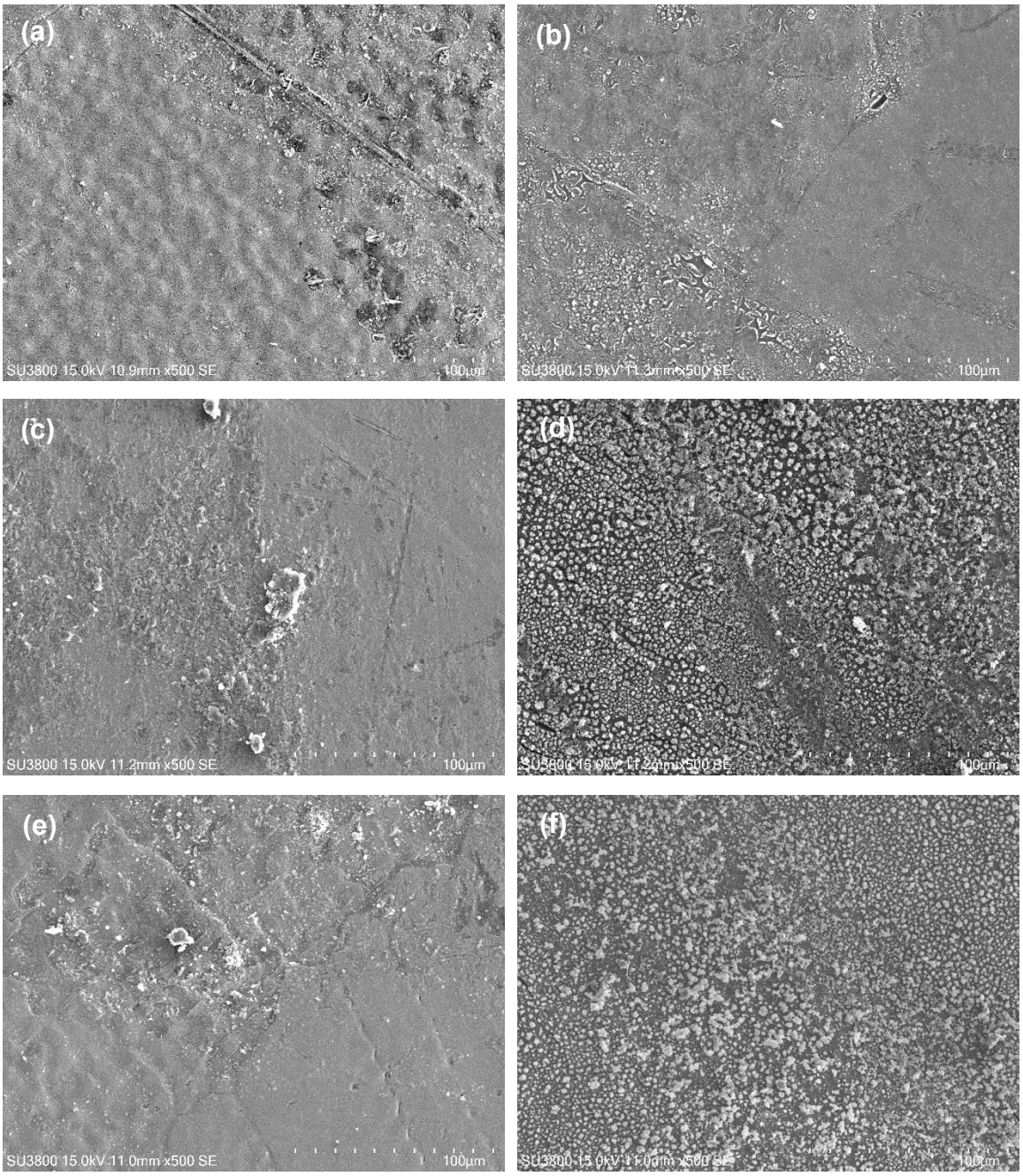

Figure 33 Surface morphology of HDG coupons exposed to: a) gas only for one week, b) gas only for one month, c) gas plus salty ash for one week, d) gas plus salty ash for one month, e) gas plus acidic ash for one week, f) gas plus acidic ash for one month

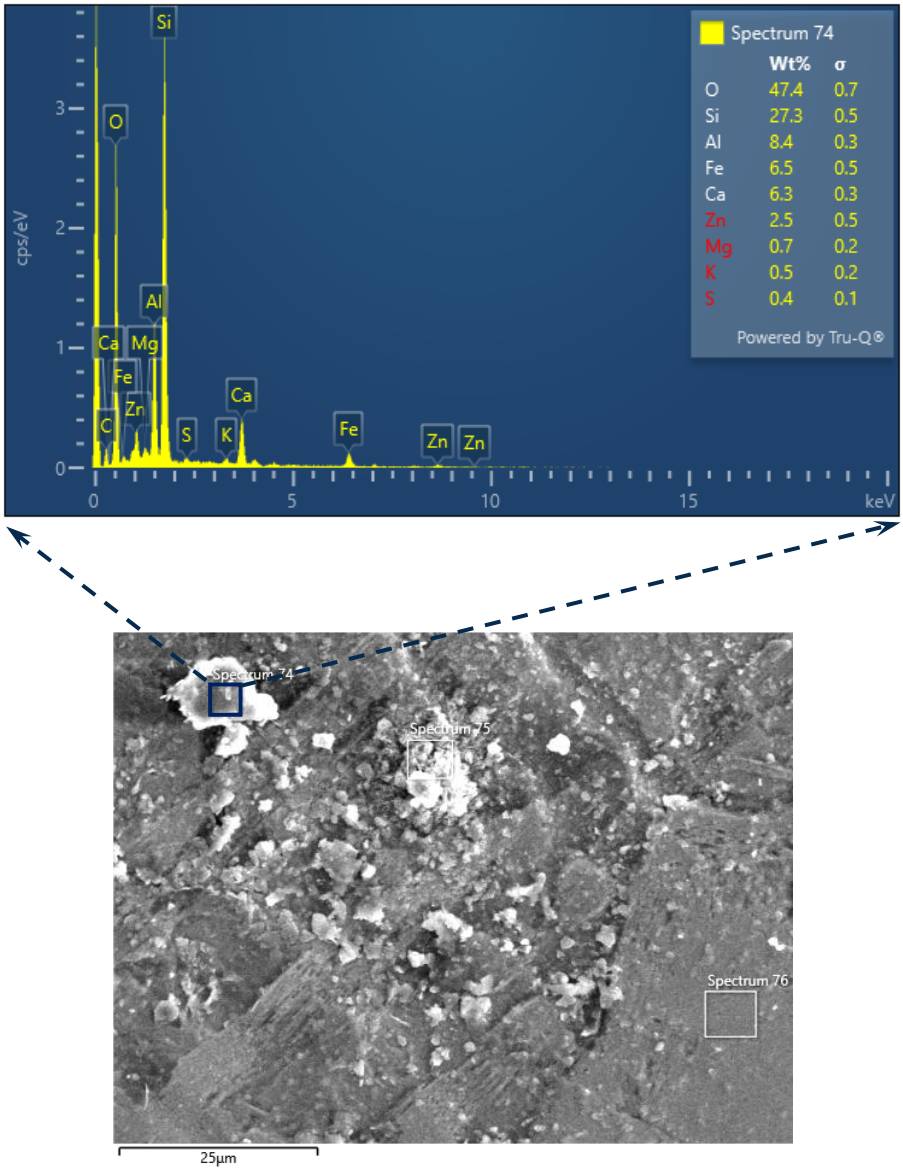

Figure 34 EDS compositional analyses of surface feature on HDG coupon exposed to gas plus acidic ash for one week

After a month of exposure, the coupon exposed to gas only was covered with a dense and uniform layer of zinc oxides and sulphides (Figure 33b), similar to findings from Li et al. (2018). Residual ash contact features were not found although it is difficult to detect the presence of ash-derived elements in the growing corrosion products. For the coupons exposed to gas plus ash (Figure 33d and 33f), surface morphology was different and surfaces were covered with small clusters of nodules. While they appeared different, EDS elemental analysis indicated that these features are also comprised of zinc oxides and sulphides (Figure 35). The corrosion rates at one, three and 12 months were very similar for all three exposures (gas only, gas plus salty ash, gas plus acid ash).

Thus, although the presence of ash could accelerate HDG coating corrosion initially, its influence was not sustained.

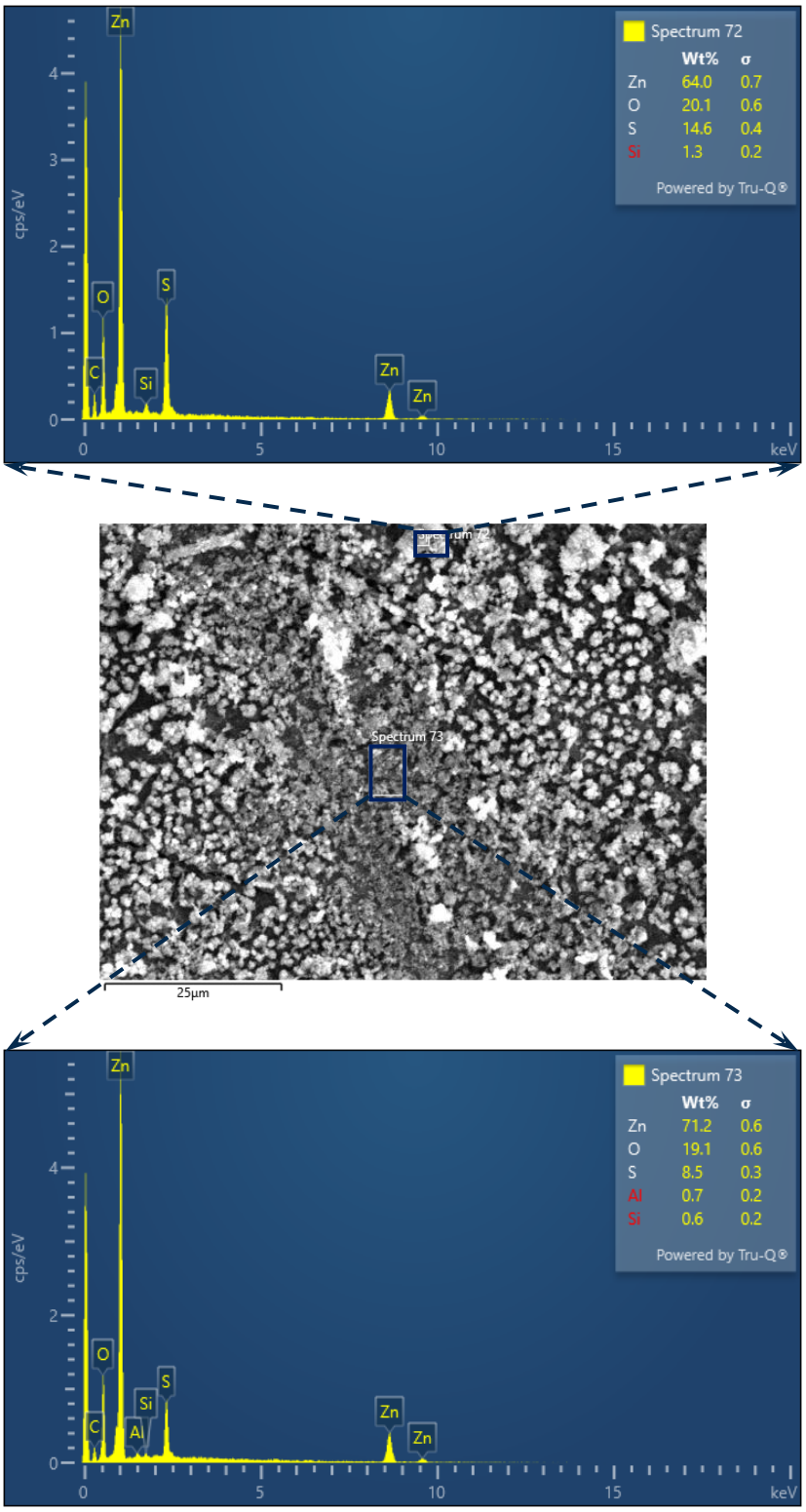

Figure 35 SEM-EDS compositional analyses of corrosion products remaining on HDG coupon exposed to gas plus salty ash for one month

When compared with carbon steel and copper, HDG zinc coating has a higher corrosion resistance and smoother surface with less anchoring points or other physical defects (e.g.

pits and crevices). Thus, ash particles are not retained on the surface, even after the surface starts to corrode.

Exposure to ash only

For coupons exposed to ash only, corrosion rates were high after the first week's exposure then dropped markedly for longer exposures and remained several-fold lower than for coupons exposed to gas.

SEM observations showed that the surfaces of HDG coupons covered with salty and acidic ash appear very similar, after 1 week and 1 month of exposure (Figure 36).

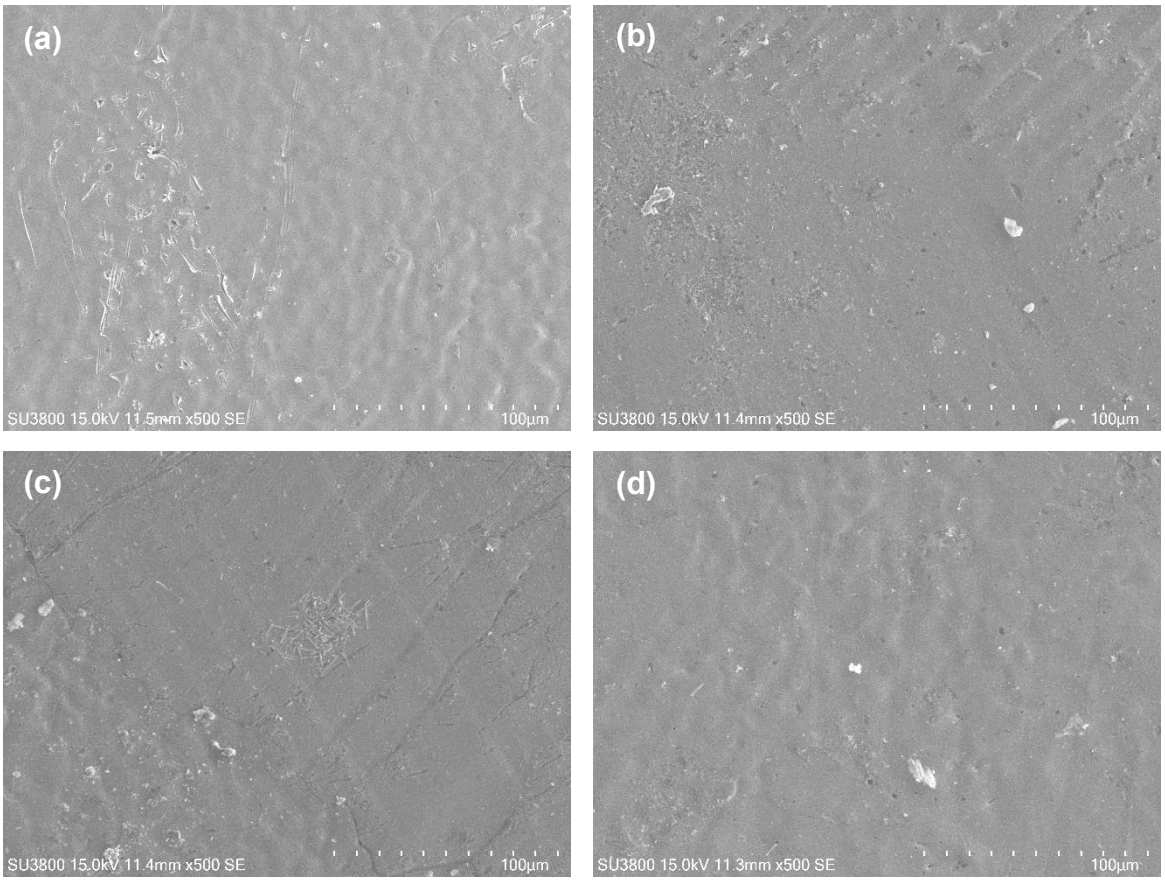

Figure 36 SEM surface morphology of HDG coupons exposed to a) salty ash only for one week; b) salty ash only for one month; c) acid ash only for one week, d) acid ash only for one month

While all surfaces appeared to be smooth and free of corrosion products in the forms of particles or clusters, SEM-EDS observations after one week of exposure revealed the presence of occasional features with the elemental signature of ash contact which may be sufficient to explain the higher initial rate of corrosion. With longer exposures, corrosion rates reduce markedly towards the baseline rate for this site (Table 8).

For longer exposures, gas is a stronger influence than ash. This may be due to the differential solubility of the corrosion products formed. In geothermal environments

products are dominated by zinc oxide / sulphide which tends to develop into clusters rather than a uniform layer (Li et al., 2018). In the absence of gas, a more continuous zinc-oxide rich layer forms which is more protective against corrosion.

Overall, ash surface coverage has an initial influence on atmospheric corrosion of HDG. Ash particles have limited interactions with the surface and are partially involved in the formation of patchy corrosion products which in turn accelerate initial corrosion rates by increasing surface roughness and attracting moisture. In the longer term, exposure to gas is more important.

Al-Zn alloy coating

Aluminium (55wt.%) - zinc alloy-coated coupons were not cleaned after field exposure to measure their corrosion rates. This is because ASTM and ISO standards have different chemical solutions recommended for cleaning after atmospheric corrosion exposure and there are arguments around their effectiveness for corrosion product removal. For this project, cleaning to calculate accurate corrosion rates was considered too difficult considering that corrosion was very limited over the duration of the study.

For this study, coupon surface conditions were characterised visually and with scanning electron microscopy (SEM).

The Al-Zn alloy coating has a microstructure that is more complex than HDG zinc coating. It has aluminium-rich dendrite and zinc-rich interdendritic regions. Silicon is also present in the microstructure as needle-like particles in the interdendritic regions. The dendrite constitutes approximately 80% of the coating volume and provides excellent long-term atmospheric corrosion resistance similar to aluminium (Shastry 2005). A previous BRANZ study showed that aluminium has a high atmospheric corrosion resistance in New Zealand's geothermal environments, even those with high concentrations of sulphur-containing gases (Li et al., 2018). As a result, when Al-Zn alloy coatings are exposed to the atmosphere, corrosion takes place preferentially in the zinc-rich region.

Gas only and ash plus gas exposures

SEM observations revealed that, in general, the surface morphologies of Al-Zn alloy coatings exposed to gas only and gas plus ash for periods of one week and one month were similar (Figure 37). There were no signs of ash particles, or of severe corrosion attack or coating damage after these short exposures.

There were some surface features resembling particles or small clusters observed only on the coupons exposed to gas plus ash (Figure 37c-387f). It was challenging to determine their composition with EDS (Figure 38) because of their small size and sparseness.

Although trace quantities of silicon were detected, we cannot differentiate silicon due to ash contact from silicon naturally present in the Zn-Al alloy coating. However, their presence only on coupons exposed to ash is indicative of interactions.

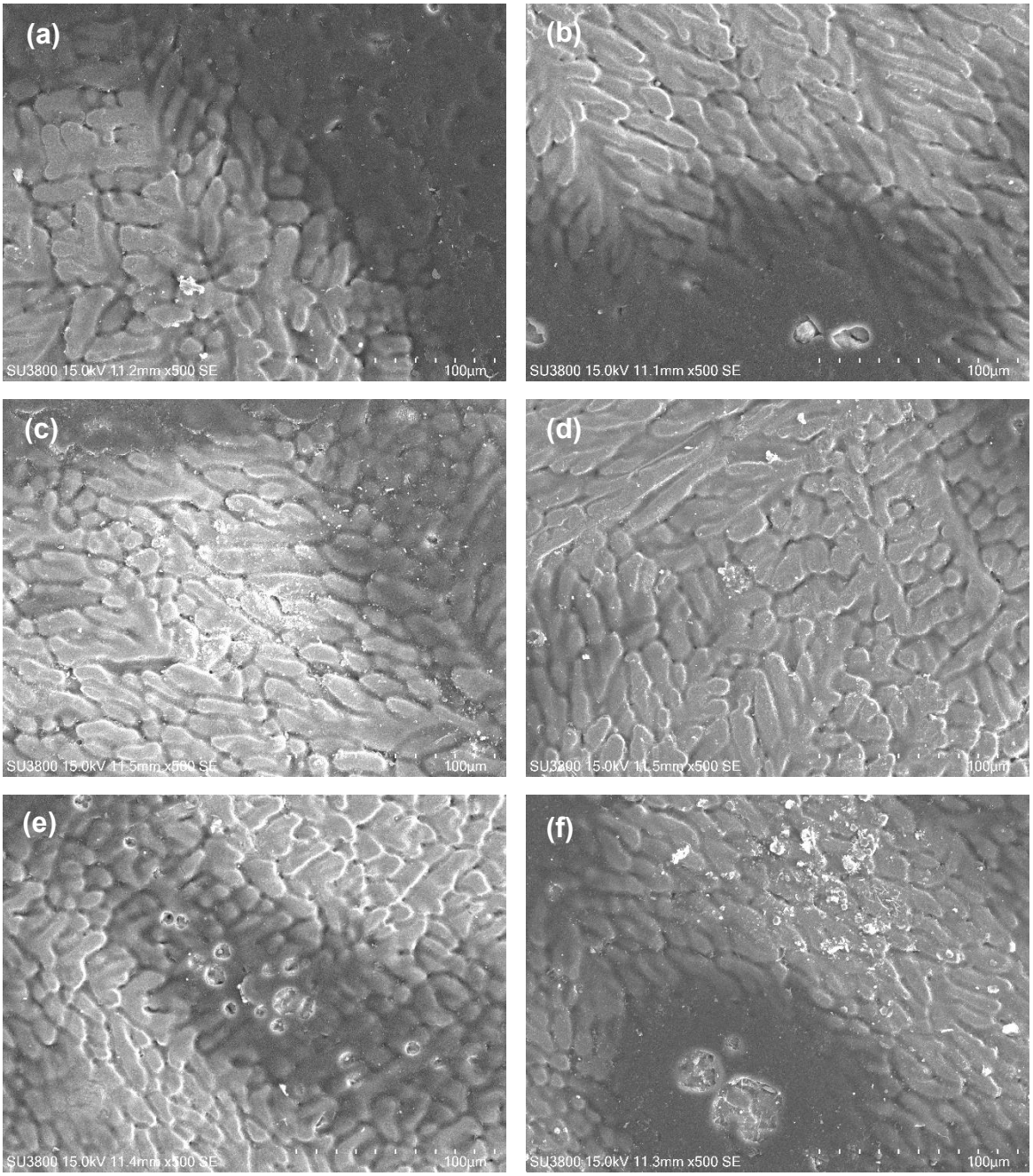

Figure 37 SEM surface morphology of Al-Zn alloy-coated coupons exposed to: (a) gas only for 1 week, (b) gas only for 1 month, (c) gas plus salty ash for 1 week, (d) gas plus salty ash for 1 month, (e) gas plus acid ash for 1 week, and (f) gas plus acid ash for 1 month.

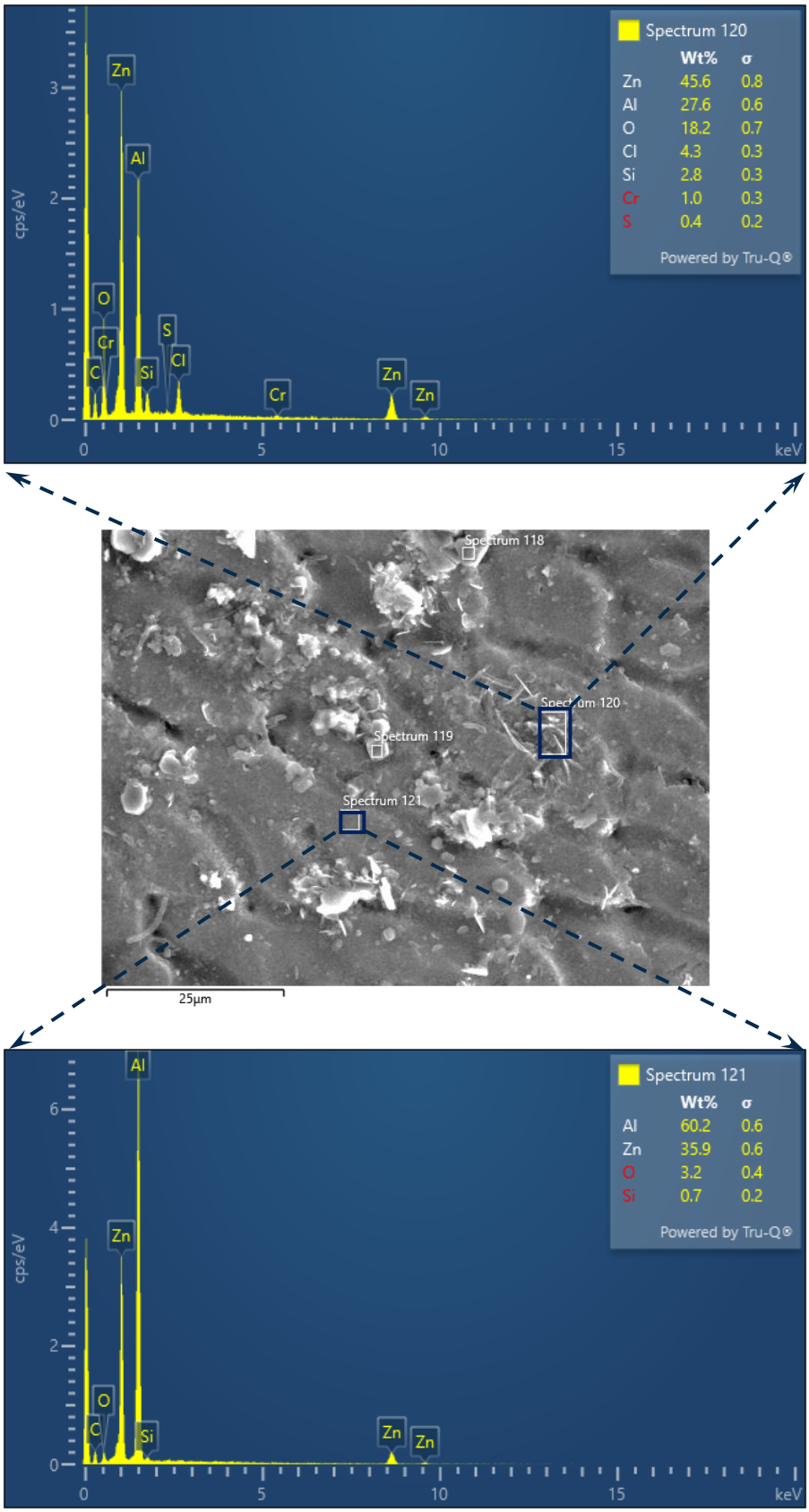

Figure 38 SEM-EDS compositional analyses of top surface features of Al-Zn alloy-coated coupon exposed to gas plus acid ash for one month

Some SEM-EDS analyses were performed for polished cross sections. Elemental mapping indicated that oxygen was rich in a small area, indicated in the yellow circle (Figure 39). This corresponds to a zinc-rich interdendritic region. While this could be evidence of preferential attack of the zinc-rich region under these exposure conditions, we cannot associate it with the presence of ash.

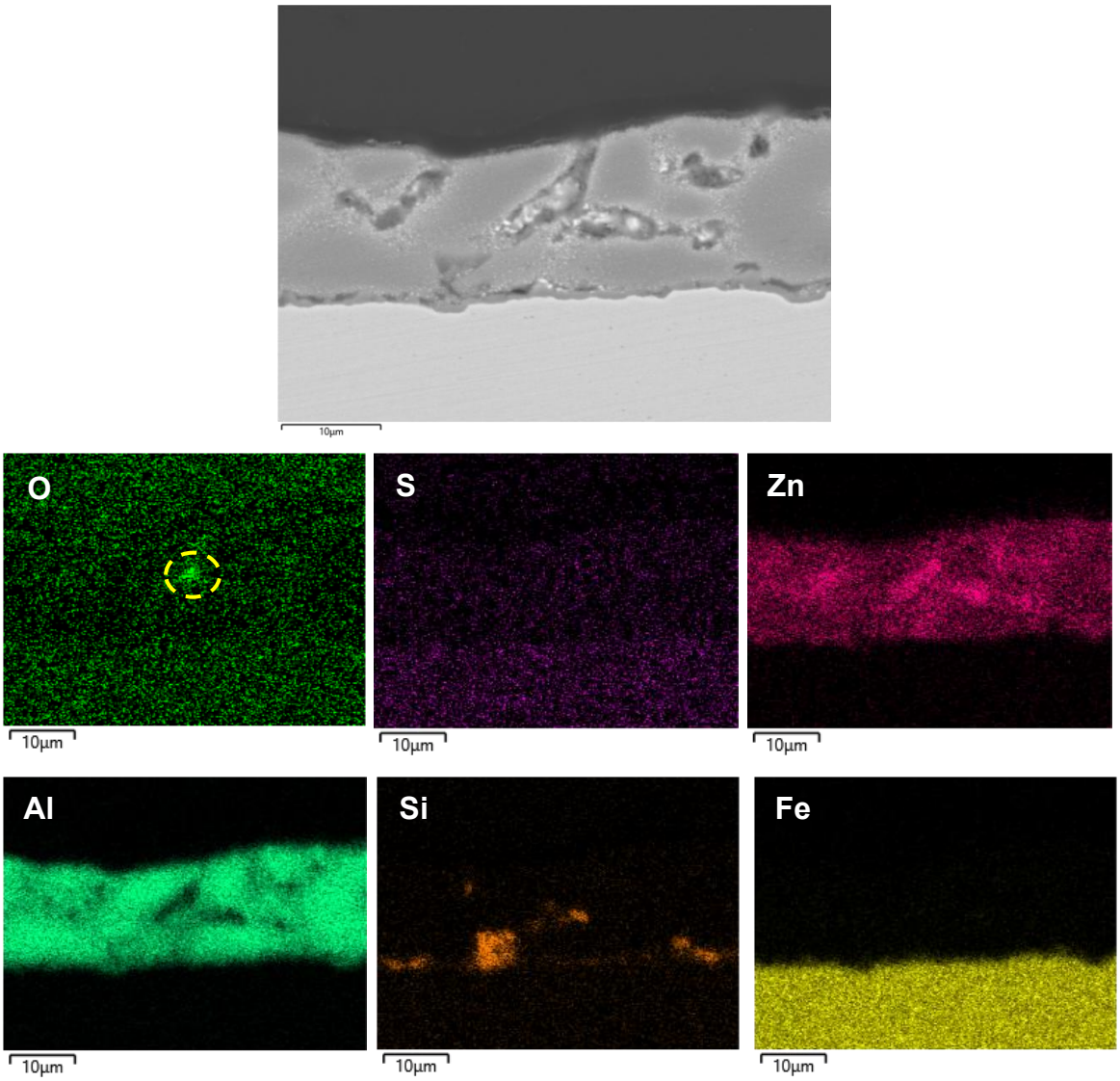

Figure 39 SEM-EDS elemental mapping of polished cross section of Al-Zn alloy-coated coupon exposed to gas plus acid ash for one month

Exposure to ash only

For coupons exposed to ash only for a week and a month, surface morphologies were similar to those exposed to gas only and ash plus gas, with no signs of ash particles, severe corrosion attack or coating damage or failure. Some surface features such as small particles or clusters were observed.

Overall, SEM morphological observations indicated that ash surface coverage may have some interactions with the surface of Al-Zn alloy coating material in the initial stages of field exposure. However, these interactions are very limited and unable to cause significant changes to the growth and evolution of corrosion products, particularly if the ash particles were washed away quickly.

Quartz-zinc

Quartz-zinc coupons are pre-weathered and their top and bottom surfaces are different. It is technically impossible to completely remove corrosion products using a specific chemical solution. As such, the only characterisation done with the coupons after field exposure was visual surface inspection.

No visible changes were observed on the surfaces of quartz-zinc coupons for any exposure conditions after three months (Figure 40). After a year, coupons exposed to gas only and gas plus ash, at the wastewater treatment plant site, showed the formation of a white powder on their top surfaces. These powdery corrosion products were loosely attached to the material surface and could be easily removed by hand wiping. Similar surface morphology and corrosion products have been commonly observed on pure zinc coupons exposed in geothermal environments (Li et al., 2018). No differences were apparent between the presence or absence of ash.

Coupons exposed to ash alone did not develop the powdery white coating even after a year’s exposure. However, the coupons were slightly darker after a year’s exposure compared to shorter exposures.

These visual surface inspections indicate that ash surface coverage may have no measurable impacts on corrosion and degradation of quartz zinc. This may be due to the naturally aged patina of quartz-zinc that improves its corrosion resistance compared to pure zinc, and that the surface of quartz-zinc is smooth and does not retain particles. No particles were visible after a week’s exposure in this study, suggesting that they were readily removed by rainfall.

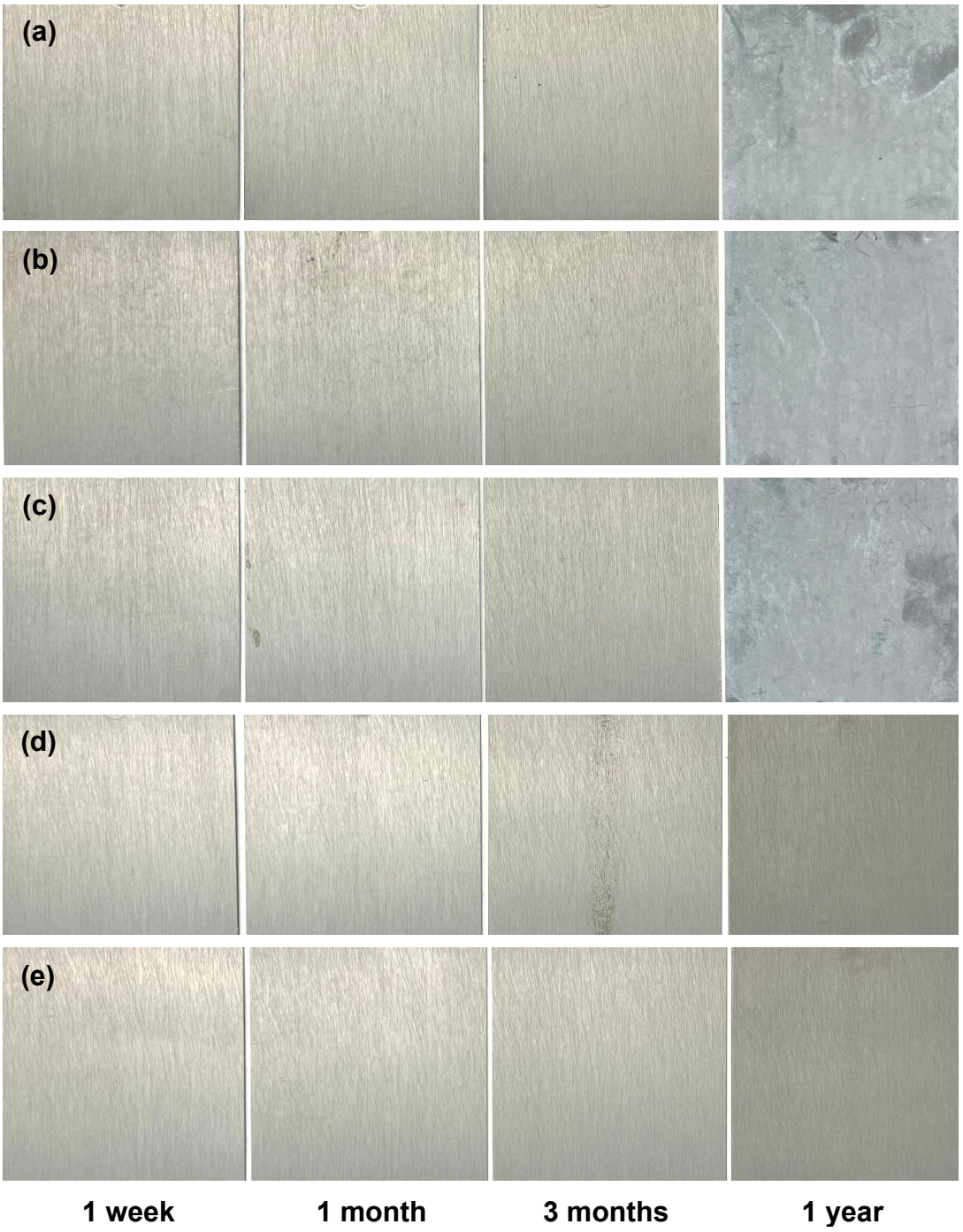

Figure 40 Visual surface conditions of quartz-zinc coupons exposed to a) gas only, b) gas plus salty ash, c) gas plus acid ash, d) salty ash only and e) acid ash only.

Limitations of study

New materials

As all test coupons were prepared from new materials, they had clean surfaces free from dirt, defects, and corrosion products. This surface condition differs markedly from that of materials in service on existing buildings and infrastructure assets. When exposed to the environment, materials begin to deteriorate at rates that depend on their inherent resistance to atmospheric attack. As degradation progresses, corrosion products form on the surface, increasing surface roughness and the effective surface area. As a result, the surface becomes more capable of retaining corrosive media from the surrounding environment, such as corrosive gases, rainwater or moisture, and ash particles. This is likely to be particularly important for materials with relatively low atmospheric corrosion resistance, such as the carbon steel examined in the present study. Rust layers containing iron oxides and hydroxides typically possess physical defects, including pores and cracks, which can trap additional corrosive media and thereby sustain or even accelerate further corrosion. Future work could investigate the performance of common building materials at different stages of weathering.

Exposure angle

The test coupons were installed at an inclination angle of 45°. This angle is widely used in atmospheric corrosion research, particularly for determining first-year corrosion rates for atmospheric corrosivity classification and for comparing the corrosion performance of different materials. However, it is significantly steeper than the roof pitches of most residential and commercial buildings in New Zealand. Typical residential roofs in New Zealand generally have slopes ranging from approximately 14° to 27° from the horizontal, although some character villas may have roof slopes exceeding 35°. Modern commercial buildings, as well as some contemporary residential buildings, often have flat or near-flat roofs with pitches below 10°. Consequently, ash particles deposited on coupons inclined at 45° can be more readily removed by rainfall, whereas ash deposits on lower-pitched roofing surfaces would be expected to remain for much longer unless removed. Future work could investigate ash adhesion to roof cladding at a wider range of angles.

Weather conditions during and after deployment

In this study, the test coupons were directly exposed to the environment and fully subjected to climatic factors. Among these, rainfall is likely to be the most critical factor governing whether, and for how long, the ash deposit layer remains on the coupon surface, particularly when surface condition and inclination angle are also considered.

Weather conditions were fine for deployment at both sites. However, rainfall commenced shortly after field deployment, with 1.6 mm recorded on the first day and 30.6 mm during the second and third days. These rainfall events removed most of the ash particles from the material surfaces. This suggests that rainfall pattern and quantity are extremely important in determining the persistence of ash deposits and their sustained corrosive effects on the underlying material. If, following a volcanic eruption, there is little or no rainfall, ash deposits may remain on material surfaces for a longer period and continue interacting with the substrate, potentially assisted by environmental moisture. Under such conditions, the corrosion process and its consequences could differ substantially from those observed in the present study. Future work could investigate the influence of weather conditions during and after ashfall on corrosion rates and processes. Rahadianto et al. (2025) note the importance of weather conditions at the time of ashfall in controlling impacts.

Volcanic ash used for testing

For this study, we used one real volcanic ash sample, from the January 2022 eruption of Hunga volcano, Tonga. However, we did not have access to sufficient quantities of real volcanic ash with an acidic leachate, so we had to reverse-engineer a bulk sample for testing purposes to create a pseudo-ash with similar acidic leachate properties to ash erupted by Ruapehu volcano in 1995/96 (Cronin et al., 1998) and Tongariro in 2012 (Cronin et al., 2014). This sample may not have been fully representative of real ash. For future ash-producing eruptions in New Zealand or potentially elsewhere, we will prioritise collecting a large bulk sample for testing purposes.

Ash deposition thickness and state

For this study we used a thin (approximately 1 mm thick) layer of ashfall dispersed across the coupons. This was primarily for practical reasons as even this quantity of ash required approximately 800 g of each type of ash. However, it is also appropriate because thin ashfalls are likely to be dispersed over a much greater area than thicker ashfalls and therefore expose more buildings (Wilson et al., 2023). We note that deposition thickness may be an important control on the rate of onset of corrosion: Oze et al. (2014) did not observe the development of corrosion for samples of weathered steel covered with 10 mm ash for a month’s exposure in an accelerated weathering chamber. Future work could investigate ash deposit thickness as a variable.

A further consideration is the state of the fresh ash deposits, which can range from dry, loose and unconsolidated to damp and clayey. Both states have been observed in ashfalls from recent eruptions in New Zealand (Figure 41). Dry, loose ash may be readily removed

by wind and rain, although in light wet weather conditions such as fog or light rain the deposit may ‘cement’ in place. Conversely, damp clayey ash is likely to stick to surfaces on buildings and other infrastructure but may dry out over time and become more unconsolidated. Future work could investigate the influence of the ashfall state on the initiation of corrosion processes.

Figure 41 Contrasting properties of fresh ashfall from two recent New Zealand eruptions. On left: fresh dry ashfall from 17 June 1996 eruption of Ruapehu, at Whakapapa village. Photo credit: P.J. Reid, Evening Post, photo purchased from Alexander Turnbull Library, Wellington. /records/22793799 On right, damp clayey ashfall from 6 August 2012 eruption of Tongariro volcano, photo credit Bubs Smith.

Conclusions

Overall, volcanic ash surface coverage can influence the corrosion behaviour and performance of metallic building materials through complex interactions between the ash, the material surface, and the surrounding environmental conditions.

For carbon steel, volcanic ash surface coverage significantly accelerated atmospheric corrosion during the initial stages of exposure. This early acceleration is likely to be associated with the influence of water-soluble ash leachates, including sulphates, chlorides, fluorides and acidity, as well as the ability of ash deposits to retain additional moisture and corrosive gases from the surrounding environment. In addition, corrosion product layers formed on carbon steel with ash coverage appeared to contain more physical defects, including vertical and horizontal cracks and pores, than those formed on carbon steel without ash coverage.

However, the effect of ash on carbon steel was not sustained over the full exposure period. Most ash particles were rapidly removed by rainfall within the first three days of field exposure, although this process is strongly dependent on weather conditions. While some ash particles were temporarily retained by the fast-growing iron-rich rust layers, these particles were progressively lost through dissolution and/or physical breakdown. As a result, after one year of exposure, the corrosion rates of carbon steel with and without ash surface coverage were very similar. The results also suggest that salty and acidic ash had broadly similar effects on the atmospheric corrosion of carbon steel.

The findings further indicate that, in the early stage of exposure, ash coverage alone can have an impact on carbon steel corrosion that is comparable to, or even greater than, exposure to gases alone.

For hot-dipped galvanised (HDG) zinc coating, ash surface coverage also accelerated atmospheric corrosion, but this effect was mainly limited to the very early stage of exposure, particularly within the first week. Interactions between ash particles and the zinc coating surface were observed at the high-gas site, although these were localised and much less extensive than those found on carbon steel. Ash coverage also made observable changes to the surface morphology of the corroding zinc coating, leading to the formation of numerous particles and/or clusters. This morphology differed from that observed on corroding zinc coating without ash coverage. For longer exposures, gas is a stronger influence than ash on rate of corrosion.

For Al-Zn alloy coating, ash particles may have interacted with the material surface during the early stage of field exposure, but these interactions appeared very limited and did not appear to significantly affect the growth or evolution of corrosion products, particularly once the ash had been rapidly removed by rainfall. Similarly, no observable detrimental effect of ash surface coverage was found for quartz-zinc under the exposure conditions investigated in this study.

In contrast to carbon steel and HDG, volcanic ash surface coverage appeared to slightly reduce the corrosion of copper when exposed to combined ash and gas. This suggests that copper is much more sensitive to corrosive gases than to ash deposition. Given the high sensitivity of copper to gas, even at relatively low concentrations, it is possible that the ash layer acted temporarily as a physical barrier, reducing direct contact between the copper surface and corrosive gases and thereby slightly slowing corrosion for a limited period.

Overall, these findings suggest that the effect of volcanic ash surface coverage is related to the inherent atmospheric corrosion resistance of the material, established in previous BRANZ studies. In general, materials with higher intrinsic atmospheric corrosion resistance are less susceptible to damage arising from ash deposition. Based on the present results, the relative sensitivity to ash influence may be ranked approximately as follows, from most to least susceptible:

carbon steel >> hot-dipped galvanised zinc coating > Al-Zn alloy coating ≈ quartz-zinc.

In this study, the influence of ash was mainly confined to the early stage of exposure, typically within the first week to first month. This was largely because most ash particles were washed away by rainfall within the first two days of field exposure. Consequently, after one year, the corrosion rates and surface morphologies of materials with and without ash coverage were generally quite similar. However, this outcome is highly dependent on weather conditions following ash deposition, as well as the condition and surface characteristics of the materials.

Overall, the findings indicate that volcanic ash should be removed from building surfaces as soon as practical and safe to do so, particularly for susceptible materials and especially where the materials are aged, weathered, or already roughened by prior corrosion.

Research benefits and future directions

This project has produced new knowledge on how volcanic ash and gas emissions can affect the corrosion behaviour and durability of metallic building materials in Aotearoa New Zealand. It addresses a significant knowledge gap, as the corrosive impacts of volcanic emissions on the built environment, particularly their combined effects, have been far less well understood than other volcanic hazards such as ash loading. By combining corrosion rate measurement, gas monitoring, and morphological / compositional characterisation, the research provides a stronger evidence base for understanding the vulnerability of buildings and infrastructure to future volcanic eruptions.

The key findings show that corrosion damage can begin immediately after ash deposition, particularly for susceptible materials such as carbon steel and, to a lesser extent, hot-dipped galvanised steel. These provide practical evidence that can support post-eruption response planning, asset management, and recovery actions aimed at limiting avoidable damage to buildings and infrastructure. This new finding replaces previous understanding (Oze et al., 2014) that onset of corrosion was not a rapid process upon exposure to volcanic ash, even on weathered materials and we note that our finding is derived from field-based testing rather than the laboratory-based testing used by Oze et al.(2014).

The comparative performance of carbon steel, copper, galvanised steel, aluminium-zinc alloy coating, and quartz-zinc under different ash and gas exposure conditions provides evidence that can inform material selection, maintenance planning, and specific engineering design in volcanic and geothermal environments. The results indicate that materials with higher inherent atmospheric corrosion resistance are generally less susceptible to the effects of ash surface coverage, while more vulnerable materials may require greater attention in design, specification, maintenance, and cleaning after ashfall. The findings can therefore contribute to future guidance, technical advice, and potentially standards-related discussions relevant to material durability and building resilience.

The findings are directly relevant to engineers, designers, building owners, insurers, territorial authorities, infrastructure operators, and communities exposed to volcanic and geothermal hazards. In particular, the work provides practical support for decision-making around the selection of durable materials, the prioritisation of ash removal, and the identification of components that may be most vulnerable after ashfall events.

By improving understanding of how volcanic emissions can damage common building materials, in both short- and long-term, this research helps strengthen preparedness and supports more effective risk communication. The evidence generated can help communities and asset owners make more informed choices before and after volcanic

events, including where to focus inspection, cleaning, repair, and replacement efforts. This is particularly important in regions where volcanic and geothermal hazards are part of the long-term risk profile, and for organisations responsible for managing buildings and infrastructure in those areas.

This research has strengthened technical capability in the area of volcanic corrosion and durability research by integrating field exposure testing, environmental monitoring, corrosion assessment, and morphological / compositional analysis. It has also supported Massey University and BRANZ to build a stronger foundation for future work at the interface of material durability, volcanic hazards, and built environment resilience. The resulting dataset, observations, and interpretations provide a valuable baseline for continued scientific investigation, sector engagement, and knowledge translation.

In the longer term, the research is expected to contribute to improved resilience of the built environment in volcanic and geothermal regions. The project has shown that material type, environmental exposure, and post-deposition conditions all influence corrosion outcomes, and that vulnerable materials can deteriorate quickly under combined ash and gas exposure. Over time, the evidence generated by this project can support more informed material choices, better maintenance strategies, improved recovery guidance, and enhanced modelling of volcanic impacts on buildings and infrastructure. These outcomes could help reduce future losses, improve recovery efficiency, and support more resilient asset planning.

This project has also identified several important next steps for future research. First, the present study used newly prepared coupons mounted at a 45° angle, and most ash deposits were removed by rainfall within the first few days of exposure. Future studies should therefore examine conditions under which ash remains on surfaces for longer periods. This includes investigating older or weathered/corroded materials, lower surface inclinations more representative of real roofs and cladding, and a wider range of post-ashfall rainfall scenarios.

Second, there is a need to extend this work beyond the Rotorua Geothermal Field to better represent volcanic eruption conditions expected elsewhere in Aotearoa. The report highlights the importance of understanding corrosion under much higher SO_2 concentrations than those encountered in Rotorua, particularly because future eruptions could generate substantially higher gas exposures over large areas. Controlled laboratory testing and/or additional field studies would help quantify relationships between gas concentration and corrosion rate and support the future development of more robust fragility functions and vulnerability models.

Third, additional research is needed to better understand mechanisms behind corrosion under combined ash and gas exposure. While this project identified clear differences in the corrosion performance of carbon steel, copper, galvanised steel, aluminium-zinc alloy coating, and quartz-zinc, some of the mechanistic explanations remain uncertain, particularly for the time-dependent behaviour of galvanised steel and the detailed role of ash in modifying corrosion product morphology and phase composition. Further microscopic, compositional analysis, and longer-duration testing would strengthen interpretation of these processes and improve confidence in practical recommendations.

Finally, uptake of the results, in the form of industry guidance, sector communications, public-facing material, and peer-reviewed publications, will help ensure that the knowledge generated by the project is applied in practice and delivers long-term benefit to exposed communities and sectors.

Publications and research outputs

New Page. Please complete the grid below to list your research outputs from the project. Provide links or send copies to Research@naturalhazards.govt.nz.

Output Type*	Date Published/ Completed	Author/s	Title	DOI or Link
Journal article	In prep	Stewart, Li, de Raadt, Tapuke	Quantifying corrosion in volcanic ash and gas environments	[to be submitted to natural hazards journal]
Journal article	In prep	Li, Stewart, de Raadt, Tapuke	Materials in extreme environments	[to be submitted to ACA journal *Corrosion and Materials*]
Industry-focused article	In prep	Li, de Raadt, Stewart, Tapuke	Performance of common building materials in volcanic ash and gas environments	[to be prepared for *BRANZ Build Magazine*]
Infographic	In prep	Li, Stewart, de Raadt, Tapuke	TBC	

We will prepare an infographic similar to the examples shown in Figure 40 to help share our findings back to interested parties in the Rotorua area as well as industry partners. These outputs have proved very popular with end users.

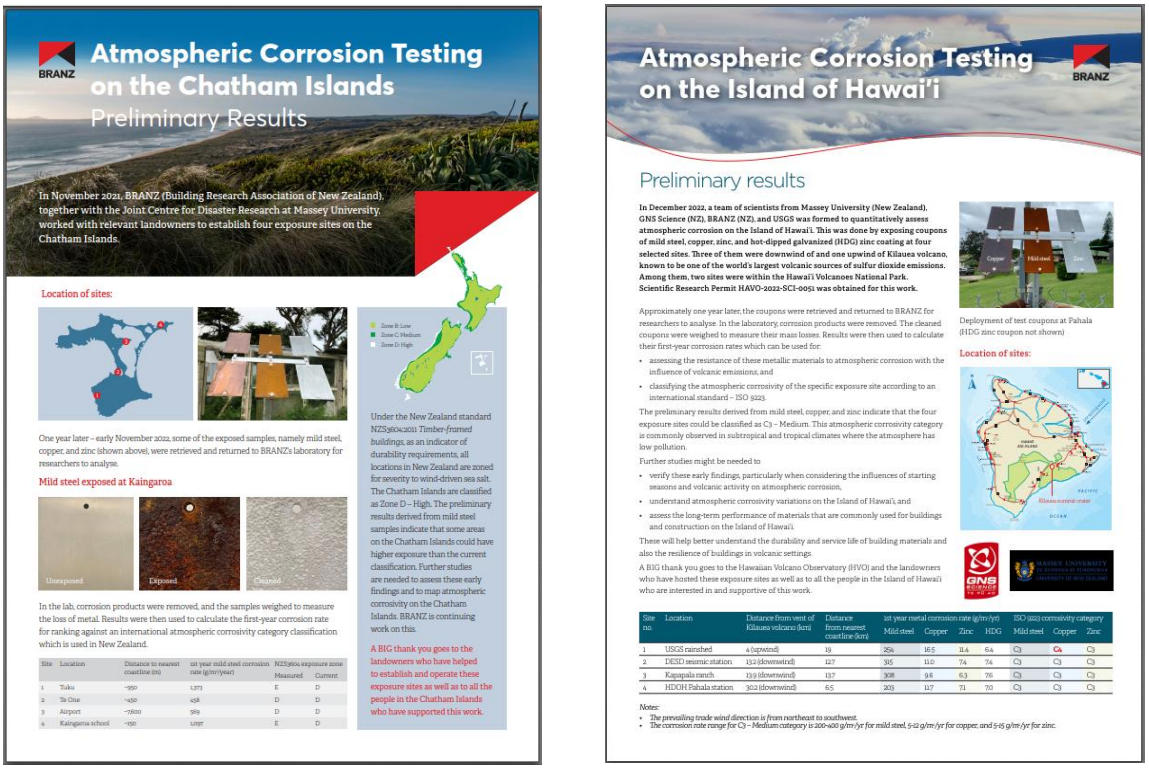

Figure 42 Examples of infographics sharing corrosion research with end users

Communications and dissemination

- Carol Stewart, Zhengwei Li, Anna de Raadt and Kelvin Tapuke. Quantifying corrosion to improve Aotearoa's built environment resilience to future volcanic eruptions. Presentation to DEVORA Annual Research Forum, 21 October 2024
- Zhengwei Li. Corrosion and Durability Research at BRANZ. Presentation delivered at Designing Durable and Sustainable Steel Structures, hosted by HERA, ACA, and SESOC, 25 September 2025, Auckland.
- Zhengwei Li, Anna de Raadt, Carol Stewart, and Kelvin Tapuke. Investigating Damage to Building Materials from Volcanic Emissions. Presentation delivered at the Ash to Action Workshop, organised by Earth Sciences, NIED, and the University of Canterbury, 3 March 2026, Rotorua.
- Carol Stewart, Zhengwei Li, Anna de Raadt and Kelvin Tapuke. Quantifying corrosion to improve Aotearoa's built environment resilience to future volcanic eruptions. Presentation to Te Awe Mapara Annual Research Wananga, 19 May 2026

Future dissemination

- Presentation at Geosciences NZ conference in Rotorua, 30 Nov-3 Dec 2026
- Presentations at future Cities on Volcanoes or IAVCEI conferences

Research team

Dr Zhengwei Li, BRANZ Ltd, Senior Scientist, co-principal investigator

Dr Carol Stewart, Massey University, Associate Professor, co-principal investigator

Dr Anna de Raadt, BRANZ Ltd, Team Leader, liaison with industry partners

Kelvin Tapuke, Massey University, Senior Research Fellow, liaison with local stakeholders

References

Bebbington, M., Stirling, M., Cronin, S., Wang, T., Jolly, G. (2018) National-level long-term eruption forecasts by expert elicitation. Bulletin of Volcanology 80, 56. 10.1007/s00445-018-1230-4

Bustaffa, E., Cori,L., Manzella, A., Nuvolone, D., Minichilli, F., Biachi, F. and Gorini, F. (2020) The health of communities living in proximity of geothermal plants generating heat and electricity: a review. Science of the Total Environment 706, 135998.

Chambefort, I. (2020) Sulfur in New Zealand geothermal systems: insights from stable isotope and trace element analyses of anhydrite from Rotokawa and Ngatamariki geothermal fields, Taupō Volcanic Zone. New Zealand Journal of Geology and Geophysics 64 (2-3), 372-377. https://doi.org/10.1080/00288306.2020.1851265

Cronin, S.J., Stewart, C., Zernack, A.V., Brenna, M., Procter, J.N., Pardo, N., Christenson, B., Wilson, T., R.B. Stewart, R.B., M. Irwin, M. (2014) Volcanic ash leachate compositions and assessment of health and agricultural hazards from 2012 hydrothermal eruptions, Tongariro, New Zealand, Journal of Volcanology and Geothermal Research, 286, 233-247.

Cronin, S.J., Hedley, M.J., Neall, V.E., Smith, R.G. (1998) Agronomic impact of tephra fallout from the 1995 and 1996 Ruapehu Volcano eruptions, New Zealand. Environmental Geology 34, 21-30.

Durand, M. and Scott, B. (2005) Geothermal ground gas emissions and indoor air pollution in Rotorua, New Zealand. Science of the Total Environment 345, 69-80.

Genareau, K., Cronin, S.J., Stewart, C., Bhattacharyya, S. and Donahoe, R. (2016) Post eruptive impacts of pyroclastic deposits from basaltic andesite stratovolcanoes on surface water composition, Journal of Geophysical Research: Biogeosciences 121, 1275–1287, doi:10.1002/2015JG003316.

Giggenbach, W.F. (1997) Relative importance of thermodynamic and kinetic processes in governing the chemical and isotopic composition of carbon gases in high-heatflow sedimentary basins. Geochimica Cosmochimica Acta 61, 3763–3785.

Haraden, J., (1991) SO_2 production rates for geothermal resources. Energy 16, 1185-1190.

Hinz, R. (2011) Hydrogen sulphide in Rotorua, New Zealand: personal exposure assessment and health effects. MSc thesis, Massey University.

Iremonger, S.D. (2004) NERMN air monitoring NOx, SOx and VOC passive sampler project 2000-2001. Environment BOP Environmental Report 2002/04.

Iremonger, S.D. (2008) NERMN Air monitoring 2007.

Kristmannsdóttir, H.,Sigurgeirsson, M., Ármannson, H., Hjartarson, H., Ólafsson, M. (2000) Sulfur gas emissions from geothermal power plants in Iceland. Geothermics 29, 525-538.

Li, Z., Marston, N. and Stokes, K. (2018) Materials within geothermal environments. BRANZ Research Report SR393. https://www.branz.co.nz/design-build/publications/sr393-materials-within-geothermal-environments

Oze, C., Cole, J., Scott, A., Wilson, T., Wilson, G., Gaw, S., Hampton, S., Doyle C., Li, Z. (2013) Corrosion of metal roof materials related to volcanic ash interactions. Natural Hazards 71, 785-802.

Rahadianto, H., Tatano, H., Iguchi, M. (2025) Multiscale impact assessment of massive ash fallout from a large eruption: what may happen if Sakurajima Taisho eruption occurs in contemporary Japan? Journal of Disaster Science and Management 1:14. https://doi.org/10.1007/s44367-025-00023-1

Siegel, S.M., Penny, P., Siegel, B.Z. and Penny, D. (1986) Atmospheric hydrogen sulfide levels at the Sulfur Bay wildlife area, Lake Rotorua, New Zealand. Water, Air, Soil Pollution 28, 385-391.

Shastry, C.R. (2005) Corrosion of metallic coated steels, in Corrosion: Materials, Vol.13B, ASM Handbook, Eds. S.D. Cramer and B.S. Covino, Jr., ASM International, www.asminternational.org, 35-39.

Vasilakos, C., Maggos, T., Bartzis, J.G. and Papagiannakopoulos, P. (2005) Determination of atmospheric sulfur compounds near a volcanic area in Greece. Journal of Atmospheric Chemistry 52, 101-116.

Wilson, T.M., Weir, A., Magill, C., Fairclough, R., Tilley, L., Liu, L., Noakes, C., Tsang, S., Kortright, N., Mace, H., Bebbington, M., Mead, S., 2023. Volcanic Hazard and Risk Assessment of the Aotearoa New Zealand Transmission Network. University of Canterbury science report prepared for Transpower New Zealand Limited. 106 pages. https://nzlifelines.org.nz/wp-content/uploads/2025/08/nva_part_c_sectors_and_hazards_v1_0_sept_2023.pdf

Appendix 1 Attempts to measure SO_2 at the wastewater treatment plant

The Rotorua geothermal field is dominated by emissions of H_2S and CO_2 (Durand and Scott, 2005). The H_2S is thought to primarily originate primarily from pyrite-bearing basement rocks (Chambefort, 2020). As the geothermal reservoirs are a chemically reducing environment, underground fluids carry sulphur entirely as H_2S and are not thought to be an appreciable source of SO_2 emissions to the atmosphere.

However, there may be minor anthropogenic sources of SO_2 from domestic home heating and diesel and coal combustion. Further, once in the atmosphere, H_2S slowly oxidises to SO_2 via the process $2H_2S + 3O_2 \rightarrow 2SO_2 + 2H_2O$ (Haraden, 1991; Kristmannsdóttir et al., 2000). To our knowledge, there is no regulatory grade data available for SO_2 in the atmosphere in Rotorua.

Data from passive samplers

We deployed passive samplers to the study site for three weeks from the deployment dates of 16-17 July 2024. This method relies on molecular diffusion and chemical adsorption. SO_2 is trapped by a chemical absorbent (triethanolamine). In the laboratory the SO_2 is extracted as sulphate ions and measured by ion chromatography. The results are shown in Table A1:

Table A1 SO_2 concentrations at WWTP site from passive diffusion tube deployment

	SO_2, µg/m^3
Tube 1	88.7
Tube 2	105.4
Tube 3	87.7
Average	93.9
Standard deviation	9.9

This is similar to values reported by Li et al. (2018) of approximately 70-85 µg/m^3 SO_2 at the wastewater treatment plant site using passive samplers. However we note that these values are not supported by the Airly sensor data prior to malfunction, nor by the expected geochemical behaviour of the Rotorua geothermal field and therefore may include positive bias associated with interference from reduced sulfur species or sulfate-containing particulates.

We note that Rotorua is globally unique in its high ambient concentrations of H_2S, and many manufacturers do not account for positive interferences from H_2S which may generate false positive signals.

Data from Airly sensor

The Airly sensor returned data for 143 days for SO_2 before malfunctioning. After restart, the SO_2 signal increased to implausibly high values and showed a strong covariance with H_2S, further supporting the likelihood of cross-sensitivity and measurement artefacts. Prior to malfunctioning, the daily SO_2 concentration data had a maximum of 27 µg/m^3 and a mean of 4.2 ug/m^3 and mostly fell within a narrow range of 3-5 µg/m^3. This method is based on electrochemical signal detection.

Aeroqual Series 500 meter

This sensor is a portable handheld data-logging device to measure gas concentrations using an electrochemical sensor. It was used during field visits and functioned reliably at the airport site and for H_2S at the wastewater treatment plant site. At the wastewater treatment plant site, the Aeroqual meter returned SO_2 concentrations in the range of 10-60 µg/m^3. However, these are likely to be false positive readings as the manufacturers report a cross sensitivity of approximately 2-3% for SO_2 in the presence of H_2S (as ppm). Based on this, false positive signals for a range of H_2S concentrations (annual average from Table 7 plus two representative higher concentrations) are shown in Table A2. This cross sensitivity is a common feature of methods based on electrochemical detection. Consequently, electrochemical detection methods for SO_2 are unlikely to be reliable in Rotorua because of the high ambient H_2S concentrations.

Table A2 False positive signals for SO_2 in presence of H_2S

µg/m^3 H_2S	False positive SO_2 signal at 2% cross sensitivity, µg/m^3	False positive SO_2 signal at 3% cross sensitivity, µg/m^3
392	15	22
1000	38	57
2000	76	114

Overall, we were unable to resolve problems caused by false positives for SO_2 in this study. A reference method may be required to provide reliable data for SO_2 concentrations in Rotorua.

Appendix 2

Table A3 Corrosion rate data from other BRANZ studies

Material	Time	Corrosion rates (g/m²/year) from this study					Corrosion rates from other BRANZ studies (g/m²/year)				
		Exposure conditions									
		Gas only	Salty ash + gas	Salty ash only	Acid ash + gas	Acid ash only	Gas only	No ash or gas			
		WWTP	WWTP	Airport	WWTP	Airport	WWTP	Airport	Judgeford[1]	Oteranga Bay[2]	Tuku [3]
Carbon steel	1 week	1,207	3,936	1,757	2,941	928	-	-	-	-	-
	1 month	1,496	3,794	880	3,425	686	2,251	487	393	1,449	-
	3 months	1,935	4,114	429	3,857	400	2,119	305	338	1,120	-
	12 months	3,303	3,547	272	3,386	242	1,888	199	186	433	1,373
Copper	1 week	855	642	191	777	190	-	-	-	-	-
	1 month	785	775	132	754	138	1,015	85	22	107	-
	3 months	627	478	75	546	72	685	49	21	82	-
	12 months	273	239	40	267	46	481	33	16	35	19
Hot-dipped galvanized zinc coating (HDG)	1 week	108	188	199	241	134	-	-	-	-	-
	1 month	124	114	37	111	34	128 (Zn)	10 (Zn)	103 (Zn)	95 (Zn)	-
	3 months	92	91	37	84	32	88 (Zn)	7 (Zn)	48 (Zn)	33 (Zn)	-
	12 months	119	128	9	122	5	90 (Zn)	4 (Zn)	8 (Zn)	24 (Zn)	4

(1) Judgeford: a semi-rural environment in the Wellington region
(2) Oteranga Bay: a severe marine environment located on the southwest coast of Wellington
(3) Tuku, Chatham Island: a severe marine environment situated in the southwest region of Rēkohu/Chatham Island.

Table A4 Corrosion rates for different corrosivity categories

Classifications/zones		Carbon steel	Copper	HDG
NZS 3604[1]	ISO 9223[2]	First-year corrosion rate, g/m^2/year		
B	C2 low	10-200	0.9-5	0.7-5
C	C3 medium	200-400	5-12	5-15
D	C4 high	400-650	12-25	15-30
E	C5 very high	650-1500	25-50	30-60
	CX extreme	<1500	50-90	60-180

1 https://www.standards.govt.nz/shop/NZS-36042011

2 https://www.iso.org/standard/53499.html

Table A5 Corrosivity classifications of sites from this study and other BRANZ studies

Site	Exposure conditions	ISO 9223 corrosivity		
		Carbon steel	Copper	HDG
Rotorua WWTP	Gas only	CX	CX	CX
	Gas plus salty ash	CX	CX	CX
	Gas plus acid ash	CX	CX	CX
Rotorua airport	Salty ash only	C3	C5	C3
	Acid ash only	C3	C5	C3
	No ash or gas	C2	C5	C2
Judgeford, Porirua	Semi-rural, inland	C2	C4	C3
Oteranga Bay, Wellington	Severe marine	C4	C5	C4
Tuku, Chatham Islands	Severe marine	C5	C4	C2